Fluid-structure interaction of bio-inspired flexible slender structures: A review of selected topics

Chenglei Wang [a)] Hui Tang [a)] Xing Zhang [b) c) *]

a) Research Center for Fluid Structure Interactions, Department of Mechanical Engineering, The Hong Kong Polytechnic University, Kowloon, Hong Kong SAR, China
b) The State Key Laboratory of Nonlinear Mechanics (LNM), Institute of Mechanics, Chinese Academy of Sciences, Beijing 100190, China
c) School of Engineering Science, University of Chinese Academy of Sciences, Beijing 100049, China

[*] Corresponding author: zhangx@lnm.imech.ac.cn

Abstract

Flexible slender structures are ubiquitous in biological systems and engineering applications. Fluid-structure interaction (FSI) plays a key role in the dynamics of such structures immersed in fluids. Here we survey recent studies on highly simplified bio-inspired models (either mathematical or mechanical) that aim at revealing the flow physics associated with FSI. Various models from different sources of biological inspiration are included, namely, flexible flapping-foil inspired by fish and insects, deformable membrane inspired by jellyfish and cephalopods, beating filaments inspired by flagella and cilia of microorganisms, and flexible wall-mounted filaments inspired by terrestrial and aquatic plants. Suggestions on the directions for future research are also provided.

Keywords: fluid-structure interaction; flexibility; flapping foil; jellyfish swimming; ciliary propulsion; plant motion in fluid; energy harvesting

1. Introduction

The interactions of fluid flows with flexible structures are omnipresent in biological systems and biology-inspired designs. In nature, fish and bats propel themselves by bending their fins or wings; jellyfish and squids utilize body contraction and expansion for propulsion; microorganisms locomote in fluids through the beating of cilia or flagella; stalks and leaves in trees experience reconfiguration when subjected to wind load. Understanding the flow physics of such interactions is important for fundamental research as well as biomimicry engineering.

Since this topic is very broad and impossible to be reviewed within one single paper, the present review selectively covers the literature of fluid mechanics studies that are inspired by macroscopic/microscopic bio-locomotion and plant motion in fluids. For bio-locomotion, three types of propulsion are included, i.e., flapping-based propulsion utilized by fish, jetting- and paddling-based propulsion utilized by jellyfish and cephalopods, and ciliary propulsion utilized by microorganisms. We review theoretical, experimental and numerical studies on highly simplified mathematical (or mechanical) models (in terms of geometry, material property and actuation pattern). The aim of those works is to reveal the flow physics rather than to mimic the intricate structures and functions of complex biological systems. Several types of simplified models and their corresponding sources of biological inspiration are summarized in Figure 1.

Further restrictions are applied on the selection of papers for review. We only focus on flexible slender structures. Here the term 'slender' means that the length-scale in one dimension is much smaller than those in other dimensions. Some interchangeable words found in the literature to describe the structures of this type include flap, filament, plate, membrane, panel etc. The term 'flexible' means the structures belong to deformable continua. Not reviewed here are the studies on rigid flapping foils or rigid flapping foils linked by torsional springs (i.e., structures with torsional flexibility). Other unreviewed systems include non-motile flagella and cilia serving as sensory organelles for sensing chemical and mechanical gradients [1].

We realize that there exist some excellent reviews whose scopes partially overlap with that of this paper. For example, reviews on flapping bodies interacting with fluids [2-6], plant-flow interactions [7-9], ciliary propulsion and flexible fibers in low-Reynolds flows [10-12], just to list a few. Readers are referred to these references for more comprehensive surveys of specific fields.

The rest of the paper is organized as follows. Section 2 introduces the studies related to bio-locomotion of macroscopic scale, including flexible propulsors inspired by insects, fish, jellyfish and cephalopods. Section 3 reviews the studies related to bio-locomotion of microscopic scale. Section 4 presents the studies on wall-mounted flexible structures inspired by terrestrial and aquatic plants. Section 5 covers the studies on flow energy harvesting using eel-like flexible slender structures. Recommendations for future research directions are provided in Section 6.

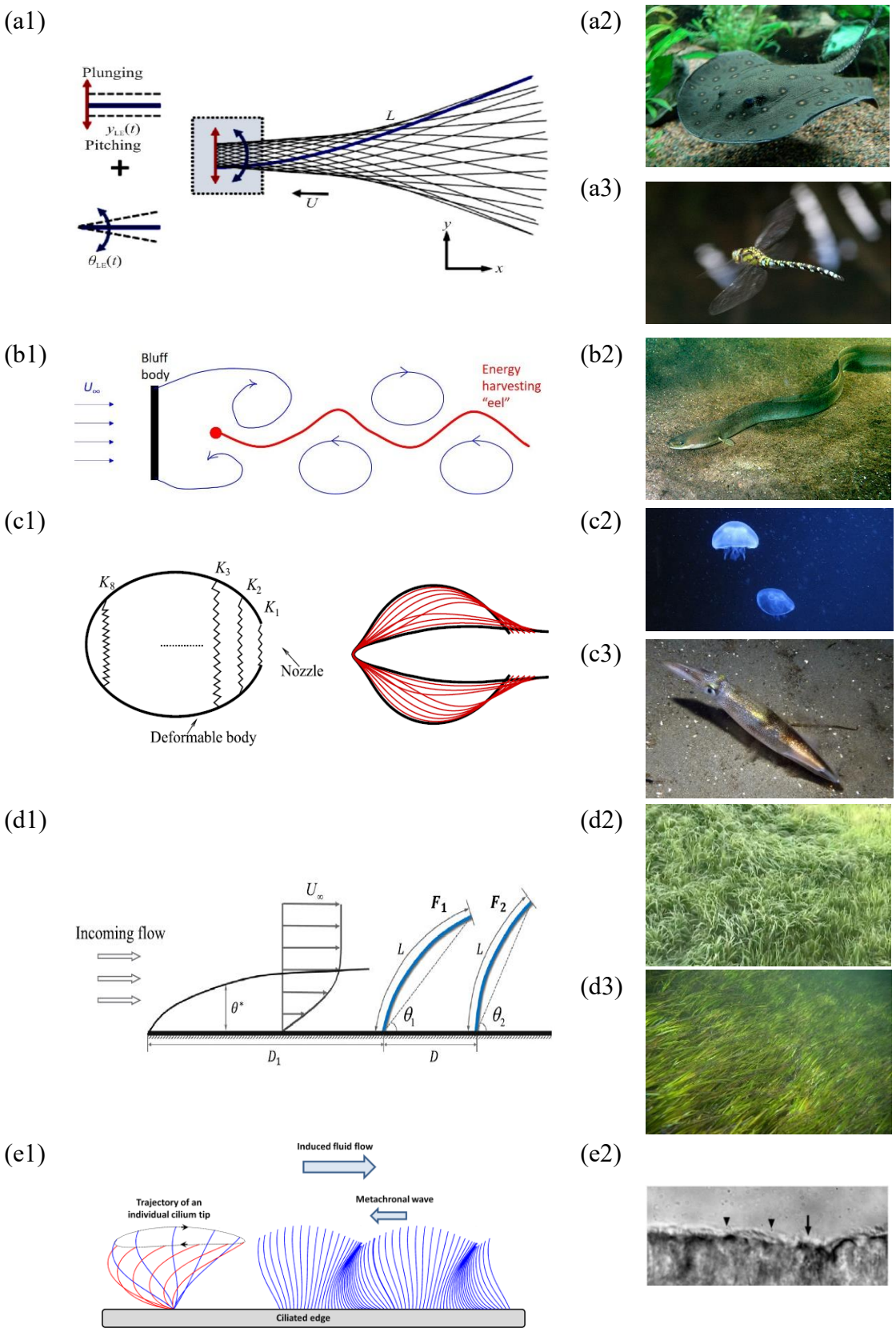

Figure 1 Simplified physics models and corresponding sources of inspiration from biology. (a1) Flexible flapping foil inspired by fish and insects, and the schematic diagram is reproduced from [13] with the permission of Springer Nature; (a2) stingray [14] (CC BY-SA 3.0); (a3) dragonfly [15]

(CC BY 2.0); (b1) Energy harvester inspired by eel; (b2) eel [16] (CC BY-SA 3.0); (c1) Deformable filament inspired by jellyfish and squid, and the schematic diagram is reproduced from [17] with the permission of AIP Publishing; (c2) jellyfish [18] (CC BY 3.0); (c3) squid [19] (CC BY-SA 3.0); (d1) Wall-mounted flexible filaments inspired by terrestrial and aquatic plants, and the schematic diagram is reproduced from [20] with the permission of Elsevier; (d2) grass (by Chenglei Wang); (d3) seagrass [21] (CC BY 2.0); (e1) Schematics of the beating pattern of a flexible filament [22] (CC BY 4.0), inspired by (e2) epithelial cilia exhibiting metachronal waves [23] (CC BY 4.0).

2. **Macroscopic bio-locomotion**

The locomotory organs of some animals can be regarded as flexible slender structures. Recent investigations indicate that both active and passive flexibilities in the locomotory organs play an important role in animal propulsion [24]. Motivated by a thorough understanding of how flexibility improves the performance of natural propulsors, lots of attention have been paid to the flapping dynamics of flexible slender structures. Here we focus on two types of macroscopic propulsors, namely, flapping-based and jetting-based.

2.1. Flexible flapping foils inspired by fish and insects

A flapping foil that undergoes plunging or pitching motion (or both) with a single-point actuation is a standard model for studying the aerodynamics of flying insects and hydrodynamics of swimming fish.

The interaction between fluids and flapping foils with *active* flexibility can be regarded as a one-way coupling problem in which a known flexure is superimposed with the rigid-body driving motion. There existed a few studies in which the propulsion performance of a flapping foil with *active* flexibility was investigated. For example, Miao and Ho [25] numerically investigated the aerodynamics of a plunging airfoil with a prescribed chordwise deformation. The influence of the flexure amplitude on the propulsion performance has been comprehensively examined.

A more challenging task is to understand the role *passive* flexibility plays in locomotion. Unlike active flexibility, two-way coupling between fluid and structure has to be considered in studies involving passive flexibility.

Some studies were motivated by the aerodynamics of flying animals and thus the emphasis was placed on how flexibility affected the generation of lift [26-31]. Yin and Luo [26] carried out a two-dimensional numerical study on a deformable flapping foil in hovering flight. They found that both the inertial- and flow-induced deformations can result in lift enhancement, and the latter can also lead to higher power efficiency. Dai et al. [27] performed three-dimensional simulations on an elastic rectangular wing undergoing pitching motion in hovering flight. It was shown that the aerodynamic performance can be significantly affected by the amplitude of passive pitching and phase difference between passive and prescribed pitching motions. Shoele and Zhu [28] used a two-dimensional computational model with nonuniform flexibility to represent insect wing with an embedded skeleton. Their results indicated that wings with strengthened leading-edge can produce higher lift while maintaining high efficiency. Tian et al. [29] conduced a two-dimensional simulation to investigate the effect of wing flexibility in forward flight. Their results indicated that wing deformation can enhance thrust without sacrificing lift. Cleaver et al. [30] showed that spanwise flexibility can

also significantly increase the time-averaged lift of plunging wings with high or low aspect ratios. Masoud and Alexeev [31] studied the hovering aerodynamics of flexible plunging wings by using three-dimensional numerical simulations. They found that the lift and efficiency of lift production can be greatly enhanced when the wings were driven at the resonant frequency.

The largest proportion of literature was concerned with the relationship between passive flexibility and swimming performance. Note that the metrics for quantifying swimming performance are different for tethered and self-propelled swimmers. For tethered swimmers, the propulsive force and Froude efficiency are used as two metrics. For self-propelled swimmers, the cruising speed is one metric, while ambiguity still exists in the assessment of efficiency [3]. A commonly used metric for efficiency of such systems is the cost of transport (COT), i.e., energy consumption per unit mas per unit distance travelled.

In some studies, dimensional analysis was used to unveil the scaling laws for the performance of flexible flapping foils. By using energy balance arguments, Kang et al. [32] deduced a relationship which linked the thrust coefficient with effective stiffness (rigidity normalized by fluid pressure) and a dimensionless parameter which characterized the wing-tip deformation. Dewey et al. [33] derived the scaling laws for thrust and efficiency in flexible pitching panels with different aspect ratios. It was found that experimental data collapsed well only if the characteristic elastic force and the characteristic fluid force were used for the scaling in the flexible regime and the rigid limit regime, respectively. Quinn et al. [34] then extended the work by Dewey et al. [33] in several directions, i.e., heaving oscillation, multiple flow speeds, self-propelled condition and wider range of flexibility.

In some parametric studies on the flexible flapping-foil systems, the influences of stiffness, mass ratio, planform, phase lag between pitching and heaving actuations, etc., were investigated separately or combinatorially [13, 35-65]. Among these works, a unanimous conclusion is that some degree of flexibility (both chordwise and spanwise) can be beneficial for improving propulsive performance (in terms of thrust, cruising speed and efficiency). One debatable issue is whether optimal performance can be achieved at structural resonance. (Note that in discussions on the relation between swimming performance and structural resonance, only chordwise flexibility has been considered.)

Although the maxima in trailing-edge amplitudes were usually found near the natural frequencies, the relation between optimal performance (in terms of thrust, cruising speed, efficiency) and structural resonance is still muddled [48-65]. The existing disagreements in the literature were often rationalized by different assumptions made in the physical models. In the studies based on inviscid flow model with a small flapping amplitude, optimal performance was usually found to coincide with resonance. On the contrary, in systems with strong nonlinearities (such as viscous flow models with separation and finite flapping amplitude), optimal performance can be achieved at off-resonance points. Zhang et al. [65] argued that resonance can improve the performance only if the fluid force was dominant or at least comparable with the inertia force (i.e., when the mass ratio was not too large). Finally, it should also be reminded

that due to the nonlinear effect in coupled fluid-structure systems, care must be taken in evaluating the natural frequencies [56, 66].

Besides the controversy over structural resonance, some attention were also paid to the relationship between propulsive performance and wake resonance. The concept of wake resonance was first introduced in Triantafyllou et al. [67], where linear stability analysis was performed on time-averaged velocity profile behind a two-dimensional *rigid* pitching foil. They found that best propulsive efficiency can be achieved if the driving frequency matched the 'resonant' frequency of wake (i.e., the frequency of maximum amplification). The Strouhal number (dimensionless frequency) determined by using this principle was found to lie in the range for natural flyers and swimmers. The wake resonance theory was then re-examined in the flexible propulsors [68-70] and the correlation between wake stability properties and swimming performance was also confirmed. However, Arbie et al. [71] recently argued that this theory was only valid in the wakes of thrust-producing type. For momentumless wakes behind self-propelled bodies, however, the applicability of this theory was questionable.

Another research topic which attracted some attention was the influence of flexibility on wake symmetry properties [72-75]. Marais et al. [72] first reported that flexibility can inhibit the symmetry breaking of the reverse Karman vortex street behind a pitching foil. The suppression of wake deflection by flexibility was later showed by Zhu et al. [73] in flexible heaving foils under the self-propelled condition. They demonstrated that wake deflection can be enhanced by a higher degree of foil flexibility. The two opposite effects of flexibility on wake symmetry properties are illustrated in Figure 2. Shinde and Arakeri [74] showed that the flexibility in pitching foil can also suppress wake deflection and meandering in the limiting case with zero free stream. Kim and Lee [75] found that for both rigid and flexible heaving foils, the transition between symmetric and asymmetric wake patterns occurred when the sum of leading- and trailing-edge circulations reached a critical value.

More recently, additional complexities were introduced to the standard flapping-foil model, e.g., nonuniform or time-dependent flexibility [76-81], confinement imposed by ground or sidewall [82, 83], non-sinusoidal or intermittent actuation [84-87], flow-mediated interactions among multiple members [88-93], hydrophobicity in the body surface [94, 95]. These works provided physical insights into some feasible strategies that can be adopted for improving the swimming performance.

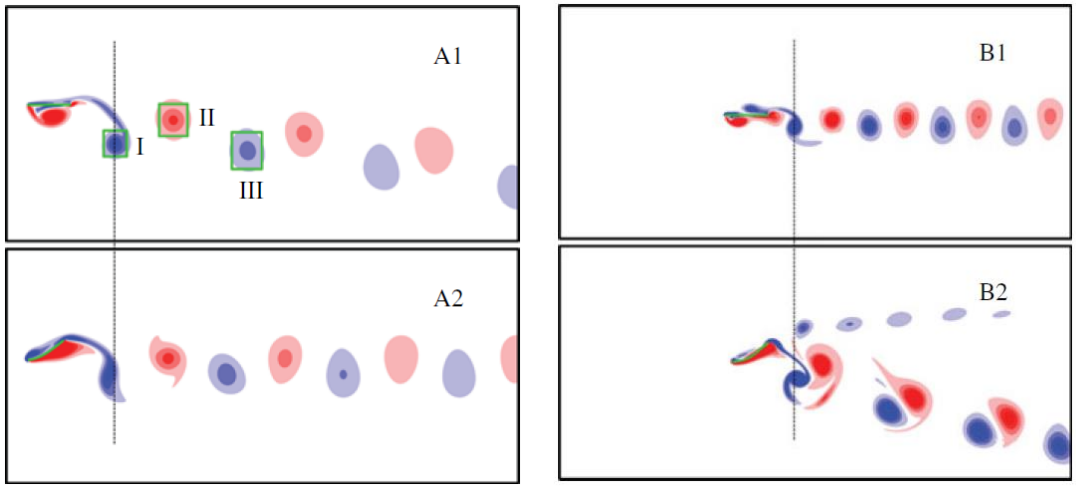

(a) (b)

Figure 2. The two opposite effects of passive flexibility on symmetry properties of the wake behind a self-propelled flapping foil. (a) Flexibility suppresses wake symmetry-breaking. Top: rigid foil; bottom: flexible foil. (b) Flexibility triggers wake symmetry-breaking. Top: rigid foil; bottom: flexible foil. Reproduced from [73], with the permission of Cambridge University Press.

2.2. Deformable structures inspired by jellyfish and cephalopods

The swimming of jellyfish and cephalopods is another mode of aquatic locomotion in which periodic body contractions are used for propulsion. Such locomotion style can be further categorized into two subtypes, namely, jetting-based and paddling-based. The former one is performed by jellyfish with prolate bell shapes, squids and octopuses, which swim via expelling a strong jet of fluid. The latter one is performed by jellyfish with oblate bell shapes, which swim via paddling motion on the bell margin. Various mathematical models with different levels of complexity have been proposed to investigate the swimming performance of such locomotion style. Although the body of jellyfish or cephalopod may not be regarded as a slender structure, the simplified models usually take the form of a filament or a membrane, which meets the defined criteria of a slender structure. Similar to the flapping-foil systems, different metrics are used for quantifying the performances of tethered and self-propelled swimmers.

The simplest physical model is a thin filament (or a membrane) whose deformation is produced solely by *active* flexibility (which mimics the muscle contraction) [96-101]. Peng and Alben [96] numerically investigated the influences of shape and stroke parameters on the performance of an axisymmetric swimmer. It was found that prolate swimmers with high stroke amplitudes were able to swim faster but with a higher energy cost. Contrarily, oblate swimmers with low stroke amplitudes were able to achieve higher efficiency but swam slower. Alben et al. [97] investigated the relationship between kinematics and performance of jetting-based swimming by using a combined computational and analytical approach. It was found that high efficiency can be achieved when the bell radius was a nearly linear function of time, or when the intermittent actuation style was adopted. Herschlag and Miller [98] used a two-dimensional jellyfish model and numerically explored the Reynolds number (Re) limit on the swimming performance. It turned out that when Re <10, the cruising velocity

decayed rapidly and the work required increased significantly, for both jetting-based and padding-based locomotion. Bi and Zhu [99] numerically studied the locomotion of an axisymmetric cephalopod-inspired swimmer based on the potential-flow framework. The free-swimming body was driven by repeated deflation-inflation cycles and swam in a bursting-coasting style. It was found that the optimal speed coincided with the critical vortex formation number. They also investigated the thrust generation of an axisymmetric deformable body via pulsed jetting [100]. In this model, both the body deformation and jet speed were prescribed. The vortex ring formation with different jet speed profiles were compared and three distinctive sources of thrust generation were identified. Luo et al. [101] extended the work by Bi and Zhu [100] by conducting a three-dimensional simulation and investigated the effect of background flow on the vortex formation and thrust generation.

More complex models that take the *passive* flexibility into account were also proposed [17, 102-109]. In Park et al. [102] [103], simulations were conducted on three-dimensional models for oblate and prolate jellyfish, respectively. They examined how the vortex structures were connected with the swimming mechanism and propulsion efficiency. Park and Sung [104] studied the interaction between two tandem self-propelled oblate jellyfish models. It was found that the flow-mediated interactions resulted in stable configurations, increase of cruising speed and reduction of cost. Hoover and Miller [105] considered the FSI problem of a two-dimensional model jellyfish bell driven at the frequency ranging from below to above its resonant frequency. It was confirmed that driving the jellyfish near the resonant frequency can result in a significant increase in cruising speed. Hoover et al. [106] developed a three-dimensional jellyfish model and studied how the swimming performance was affected by the strength of contraction and the flexibility of the bell margin. They demonstrated that flexible margin and sufficiently strong active contraction were the two key factors for fast swimming at low costs. They stepped further to confirm that the three-dimensional jellyfish model reached the maximum speed when it was driven near the natural frequency [107]. However, if high efficiency (or low COT) was given the priority, the bell should be driven below the natural frequency. Dawoodian and Sau [108] performed three-dimensional simulations to study the swimming and prey capture of a paddling jellyfish. They found that a prolate-type jellyfish was more economical in swimming than an oblate-type jellyfish. Resonant swimming was found to help jellyfish improve energy efficiency over a wide range of applied paddling force. It was also demonstrated that the Lagrangian coherent structure analysis can provide a better understanding on predator–prey interactions. Bi and Zhu [17] proposed a two-dimensional squid-inspired inflation–deflation model and investigated its propulsive performance in the tethered mode. By conducting FSI simulations, it was found that the increase in driving frequency can result in higher thrust at the cost of reduced propulsive efficiency. It was also demonstrated that the propulsive performance can be greatly impaired if the wake was disturbed by the symmetry-breaking instability. The development of symmetry-breaking instability in the wake behind a squid-inspired swimmer is shown in Figure 3. Later, they also focused on the performance of the squid-inspired model in free swimming [17, 110]. It was seen that higher speed can be

achieved by increasing the driving frequency. However, the COT was found to rise as well. Similar to that observed in the tethered mode, in free swimming the symmetry-breaking instability was also found to have an adverse effect on the propulsive performance. In Luo et al. [109], the effect of Reynolds number on its performance has been explored systematically. It was also found that actuating at the resonant frequency may not lead to better performance (in terms of mean thrust and efficiency).

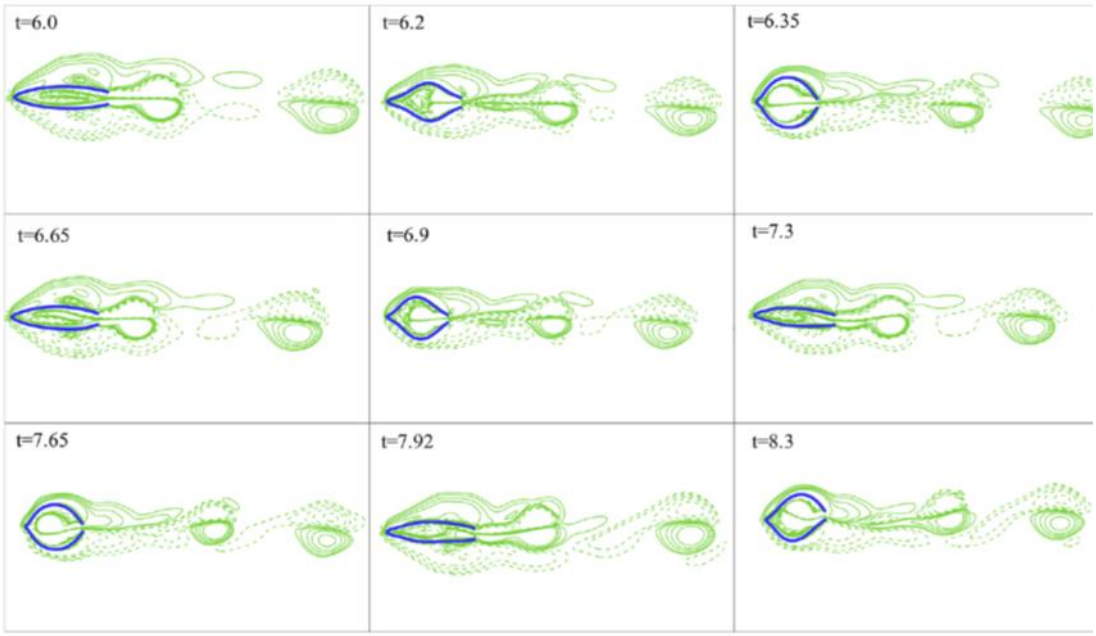

Figure 3. Development of symmetry-breaking instability in the wake and deformation of a squid-inspired swimmer. Reproduced from [17], with the permission of AIP Publishing.

3. Microscopic bio-locomotion

Flagella and cilia are micro-scale membrane-bounded organelles protruding from cell surfaces, widely existing in protists, plants and animals and serving as fundamental units of motion [12]. Their length is usually within the range of 10μm to 100μm, while their typical beating frequencies vary from 10Hz to 100Hz. As such, the Reynolds number is generally much smaller than 1, and viscous force is dominant over inertial force [111]. The length-to-diameter ratio of flagella and cilia ranges from 10 to 100 [112], which can thus be considered as slender bodies.

In general, flagella and cilia share common ultrastructure and compositions, and their internal structure called axoneme is highly conserved across evolution. Axoneme consists of arrays of microtubule doublets and thousands of dynein molecular motors [113]. In most cases, it exhibits either a “9+2” pattern composing nine doublet microtubules and a central pair of single microtubules, or a “9+0” pattern where the central pair is absent.

The spatial and temporal regulations of dynein molecular motors yield the motion of axoneme, which lead to asymmetric planar whip-like (axoneme of “9+2” pattern) or oar-like (axoneme of “9+0” pattern) beating and fluid pumping. Hence, flagella and cilia can be used for locomotion by unicellular organisms, such as sperm [114] and

Paramecium [115], or serve to break the left-right symmetry of developing embryo [116], or transport cerebrospinal fluid in brain [117] and female reproductive fluid in oviduct [118], or remove mucus in respiratory system [119]. Some creatures apply them for generating arrays of vortices for capturing preys [120], or exchanging nutrient and oxygen with the ambient fluid [121]. More functions of flagella and cilia can be found in a recent comprehensive review [122].

Although sharing the same ultrastructure and their names are often interchangeable, flagella and cilia are different [12, 123]. In practice, organelles are called flagella when they are sparsely distributed on unicellular organisms, such as sperm and the green alga *Chlamydomonas reinhardtii*, and they usually produce bending waves along their axis. By contrast, cilia refer to those that are grouped compactly and extensively in animal organs, such as the ciliated epithelial cells in human lungs, or densely anchored on the surface of protozoans, such as *Opalina*. Under this condition, they usually undergo breaststroke-like asymmetric beating motion with alternative power stroke (fast stroke with elongated shape) and recovery stroke (slow stroke with cilia bent and close to cellar surface).

3.1 Theoretical and numerical modelling

Theoretical modelling and numerical simulation have been extensively applied to reveal the hydrodynamic performance, interactions and coordination of flagella and cilia. As the flow is usually in the creeping flow regime, flagella and cilia have to break spatial-temporal symmetry to escape the scallop theorem [124] by adopting wave-like or breaststroke-like asymmetric beating motions. Even though the structural components of flagella and cilia have been identified, the mechanisms of how such components coordinate to produce asymmetric beating motions remain elusive. For effective explorations, theoretical models which are able to reproduce asymmetric motions are indispensable, the development of which is one focus of recent studies.

Some previous works developed minimal or reduced models which neglect biological complexity, i.e., the kinetics of molecular motors and the internal mechanics of axoneme. In these works, flagella and cilia are modelled as oscillators [125-128], or chains of spherical colloidal particles [112] or elastic filaments [129-131], where geometric switch schemes are adopted for actuation. Another type of models was developed by optimizing pumping efficiency of a single flagellum [130, 132] or cilia array [133], although their beating patterns could not be hydrodynamically optimal in nature [134]. By considering the effects of kinetics and dynamics of flagellar and ciliary internal structures, more realistic models have been proposed. For instance, as the internal axial stresses are sufficiently large to trigger the instability via Hopf bifurcation, it was assumed that beating flagella and cilia are driven by dynamic instability [135-137]. When the spatial and temporal regulations of dynein molecular motors are modeled based on some control schemes, such as sliding control [138], curvature control [139] and geometric clutch [113], more realistic beating patterns can be attained. It was found that the curvature-control based model is able to produce the breaststroke-like beating patterns of *Chlamydomonas* [140], while the geometric-clutch based one can generate both flagellar and ciliary waveforms [113]. By combining the sliding control and curvature control schemes, Chakrabarti and Saintillan [123] developed a

model which can exhibit various beating patterns presented in nature.

3.2 Coordination and Collective behavior of flagella and cilia

Flagella and cilia can exhibit rich dynamic behaviors when they coordinate with their neighbors. In particular, a few to hundreds of sperm can gather through mechanical coupling and display various collective patterns, such as massal motility, sperm trains and sperm bundles. The collective locomotion can yield hydrodynamic benefits [114]. For example, when two sperm get sufficiently close, their flagella can flap in phase and their beating frequency and swimming velocity can be enhanced [141]. Sperm can also exhibit collective behaviors in larger scales, including sperm vortices [142] and sperm turbulence [143]. The main factors determining the aforementioned collective behaviors have not been elucidated completely. It was found that the coordination could depend on cellular morphology [144] and concentration [142], while the adhesion may be dispensable [145]. More details about collective dynamics of sperm can be found in recent comprehensive reviews [114, 145].

As for other organisms, such as *Chlamydomonas*, each individual often has one pair of flagella which can beat in-phase and anti-phase for controlling and adjusting their swimming speed and orientation. For some other unicellular organisms, such as *Pyramimonas*, each one has multiple pairs of flagella, which usually act in group and exhibit more complex synchronization. However, the underlying mechanisms have not been fully understood, while the existing ones are sometimes controversial. Some studies found that the synchronization can arise purely from hydrodynamic interactions [125, 146], which may also cause stochastic transition from one synchronized mode to the another [131]. Quaranta et al. [147], nevertheless, suggested that the synchronization is caused by cell internal fibers which mechanically connect the flagella, whereas the hydrodynamic interaction plays a marginal role. A later study found that both these two factors, i.e., hydrodynamic interaction and mechanical connection, are essential, and their competition determines the flagellar coordination [148]. Different from the above works, Geyer et al. [149] found that "cell-body rocking" is crucial rather than direct hydrodynamic interaction.

Ciliary spatial coordination is another fantastic but more complex phenomenon. Cilia do not beat randomly, but often coordinate with their neighbors, giving rise to various metachronal waves (MCWs), including transverse (laeoplectic or diaplectic) and longitudinal (symplectic or antiplectic) waves, which are wave-like patterns with phase differences exhibiting among neighboring cilia [150, 151], as shown in Figure 1(e2). The functions of MCWs have been extensively explored in previous studies. It was found that MCWs can enhance flow transport velocity and efficiency [139] as well as fluid mixing [112], on which antiplectic wave usually outperforms symplectic one no matter cilia are immersed in one-or two-component flow [112, 152, 153]. Through an optimal-efficiency based beating model, Osterman and Vilfan [133] found that laeoplectic waves could be more efficient if cilia beat clockwise. Based on a numerical model where artificial cilia are magnetically actuated, Khaderi and Onck [154] demonstrated that laeoplectic waves inside a microchannel can create secondary flows which could be adopted for fluid mixing.

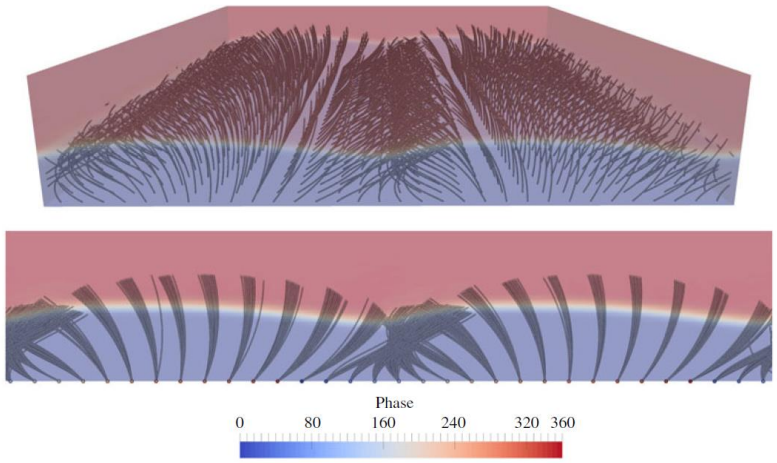

Figure 4. Longitudinal metachronal wave spontaneously emerging from hydrodynamic coupling, reproduced from [155] with the permission of Cambridge University Press.

Although their functions have been extensively investigated, the mechanisms of the emergence of MCWs remain largely unknown. Thus far, it has been found that hydrodynamic interaction can yield MCWs [129, 139, 156-161], as shown in Figure 4. For instance, Gueron et al. [156] and Elgeti and Gompper [139] showed that initially in-phase beating cilia can form MCWs after a few beating cycles via hydrodynamic interaction. However, how these interaction causes MCWs is still understudied. Some recent explorations proved that inhomogeneities can lead to wave emergence. For instance, using a minimal model, Nasouri and Elfring [162] demonstrated that the emergence of wavelike behavior of a cilia array around a sphere can arise from the difference in beating rate between one cilium and its neighbors. With a similar model, Ghorbani and Najafi [127] found that the trajectory of the cilium mass center which moves on an elliptic orbit is crucial for the emergence of symplectic or antiplectic waves, when cilia are attached to a closed body model. Through a more realistic two-dimensional model, Chakrabarti et al. [163] confirmed that one-dimensional MCWs can emerge robustly when spatial inhomogeneity is involved. Furthermore, some other factors, such as ciliary density [153], ciliary flexibility [129, 164], and biochemical noise [165], can also influence the emergence of MCWs.

Besides MCWs, other types of ciliary coordination have also been observed usually at larger scales. For instance, on coral epithelium beating cilia can generate arrays of counterrotating vortices of the size which is around hundreds of cilium length, so as to enhance nutrient and oxygen mixing with nearby fluid [121]. In cilia-mucus system reconstructed in vitro, cilia can collaboratively beat together to produce large mucus swirl whose diameter can be up to thousands of cilium length [166]. Although mechanisms of these long-range ciliary coordination remain largely unexplored, it has been demonstrated that hydrodynamic coupling could play an essential role. For example, in cilia-mucus system, it was found that such coupling could affect the two-dimensional organization of planar cell polarity (PCP) proteins, which thus dictates the coordination of ciliary beat direction [166].

4. Plant motions in air or water

Besides ciliary propulsion in microorganisms, plant-flow interaction is another source of biological inspiration for FSI in wall-mounted flexible structures. Such studies are not only crucial for agricultural and forestry production, but also have important consequences in coastal erosion control and renewable energy harvesting.

Unlike the studies dealing with locomotion, the flexible structures involved in this section are completely passive. When subjected to fluid flow, two types of reconfiguration can be found in flexible structures, namely, static and dynamic [167-175]. Static reconfiguration refers to the situation where the structures become more streamlined in shape, and therefore, the drag forces exerted on them can be reduced. Dynamic reconfiguration refers to situation where the structures oscillate in various ways. It should be stressed that in comparison with FSI studies in open space, the ones with wall confinement may involve two additional complexities. First, the existence of boundary layer completely alters the flow structures, which, in turn, affects the response of the structures indirectly. Second, the presence of wall confinement also directly hinders the movement of the structures. This may occur either through hard collision or through soft collision due to the lubrication barrier force exerted on the structures.

Henriquez and Barrero-Gil [176] investigated the static reconfiguration of a flexible plate subjected to a sheared incoming flow. Leclercq and De Langre [177] later extended this study to include the effect of structural nonuniformity. In these two works, the fluid loads on the structures were calculated using a theoretical model in which the nonuniform velocity profiles were taken into consideration.

In a series of works, Jin and coauthors experimentally investigated the interaction of wall-mounted thin plates with uniform flows at low or high turbulent levels [178-181]. Jin et al. [178] demonstrated that the frequency of the structures under streamwise motions can be decoupled from that of the wake fluctuations. Jin et al. [179] studied the influence of the tip shape on the structure dynamics and near-wake turbulence. Jin et al. [180] also investigated the coupled dynamics of two flexible plates in tandem arrangement. They found that the upstream plate always oscillated at its natural frequency, while the motion of the downstream one was significantly influenced by the vortex shedding. Jin et al. [181] focused on the dynamics of wall-mounted flexible plates under inclined flows. Three distinct modes of tip oscillation were identified with different combinations of Cauchy number and flow inclination angle.

Recently, some numerical simulations were conducted to study the FSI of wall-mounted flexible structures under a variety of configurations. In Zhang et al. [20], the interactions of single and two tandem filaments with a fully-developed laminar boundary layer were studied. The influences of bending rigidity, mass ratio, Reynolds number and gap distance on the structure dynamics and wake pattern were systematically explored. At extremely low rigidity, the lodging state (which can be regarded as one special case of static reconfiguration) was exhibited. Under certain conditions, the cavity-oscillation state (which can be regarded as one special case of dynamic reconfiguration) has been discovered in the double-filament systems. The dynamic behaviors of single and dual wall-mounted flexible filaments subjected to fluid load, together with their corresponding flow field are shown in Figure 5. In a similar

study by Wang et al. [182], the interactions of wall-mounted filaments with an oncoming Poiseuille flow were investigated. This work was then extended by Chen et al. [183] through three-dimensional FSI simulations on a single and two tandem wall-mounted flexible plates.

A few more recent studies were concerned with an array of a large number of flexible structures [182, 184-187]. In Wang et al. [182], the dynamics of the system with 50 wall-mounted filaments was explored. The transition from the static deflection mode to the flapping mode was observed when the gap distance exceeded a critical value. In Revell et al.[184], the interactions of Poiseuille and Womersley flows with an infinite series of flexible 2D filaments were investigated by imposing a periodic boundary condition. It was shown that the structure responses were significantly affected by the Reynolds number. Favier et al. [185] simulated the two-way coupled dynamics of an array of 10 filaments in a Womersley flow. They observed the waving behavior at the tips of the filaments and the formation of vortices in the gaps between the two adjacent filaments. O'Connor and Revell [186] investigated the interaction between a row of 128 filaments and a two-dimensional open-channel flow under steady-flow condition. Their results indicated that four distinct states can be identified, i.e., static, regular waving, irregular waving and flapping. The regular waving was found to occur when the frequency of the mixing layer instability and the natural frequency of the array were close to each other. Tschisgale et al. [187] performed large eddy simulations on a model submerged aquatic canopy which was made up of 800 highly flexible blades in regular arrangement. They focused on the interplay between coherent flow structures and motion of the blades. Figure 6 shows the instantaneous coherent vortex structures represented by pressure iso-surfaces. The results of this study provided an improved understanding of the wave-like motion of the canopy in streamwise direction (also known as the honami or monami phenomenon).

Some studies aiming to provide biomimicry solutions to engineering problems were also found in the literature. Inspired by the calming effect of aquatic plants, Nove-Josserand et al. [188] experimentally explored the effects of flexibility and spatial arrangement on the wave energy damping capability of an array of partially submerged flexible filaments in a water tank. Nove-Josserand et al. [189] developed a simplified one-dimensional model for the experiments presented in [188] and predicted the optimal configuration regarding energy absorption. Park [190] proposed to use a wall-mounted flexible filament as a vortex generator in a Poiseuille channel flow to improve the convective heat flux. The influences of inclination angle and bending rigidity of the filament on the thermal performance were examined. Chen et al. [191] extended the work of Park [190] by using 6 to 12 wall-mounted filaments uniformly distributed on the two channel walls. They conducted a parametric exploration to identify the effects of staggered and tandem gap distances, bending rigidity and channel height on the overall thermal performance.

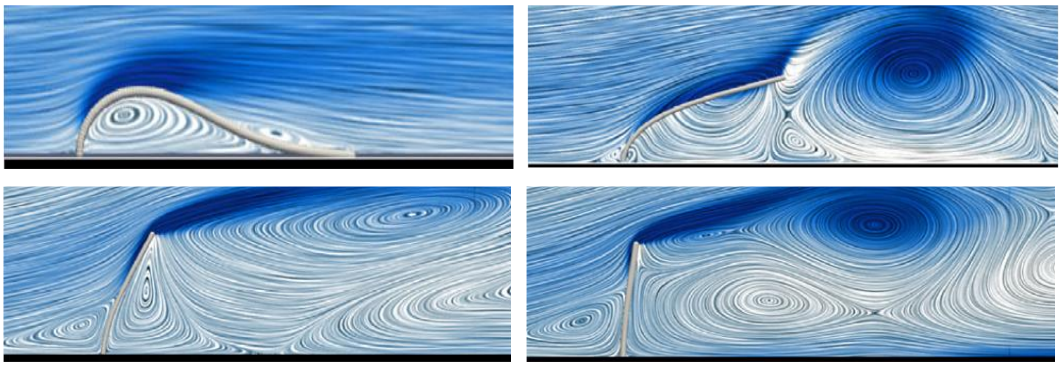

(a)

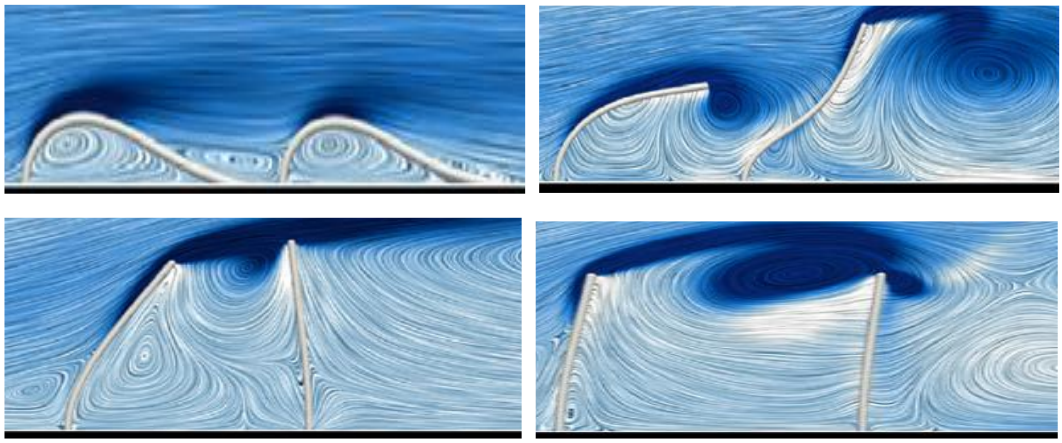

(b)

Figure 5. Dynamic behaviors of single and dual wall-mounted flexible filaments subjected to crosswise fluid flow. (a) Four typical dynamic states and flow fields for the single-filament system with different bending rigidities. Top left: lodging; top right: regular VIV; bottom left: static reconfiguration with steady flow; bottom right: static reconfiguration with unsteady flow. (b) Four typical dynamic states and flow fields for the dual-filament system with different bending rigidities. Top left: lodging; top right: regular VIV; bottom left: static reconfiguration; bottom right: cavity oscillation. Reproduced from [20], with the permission of Elsevier.

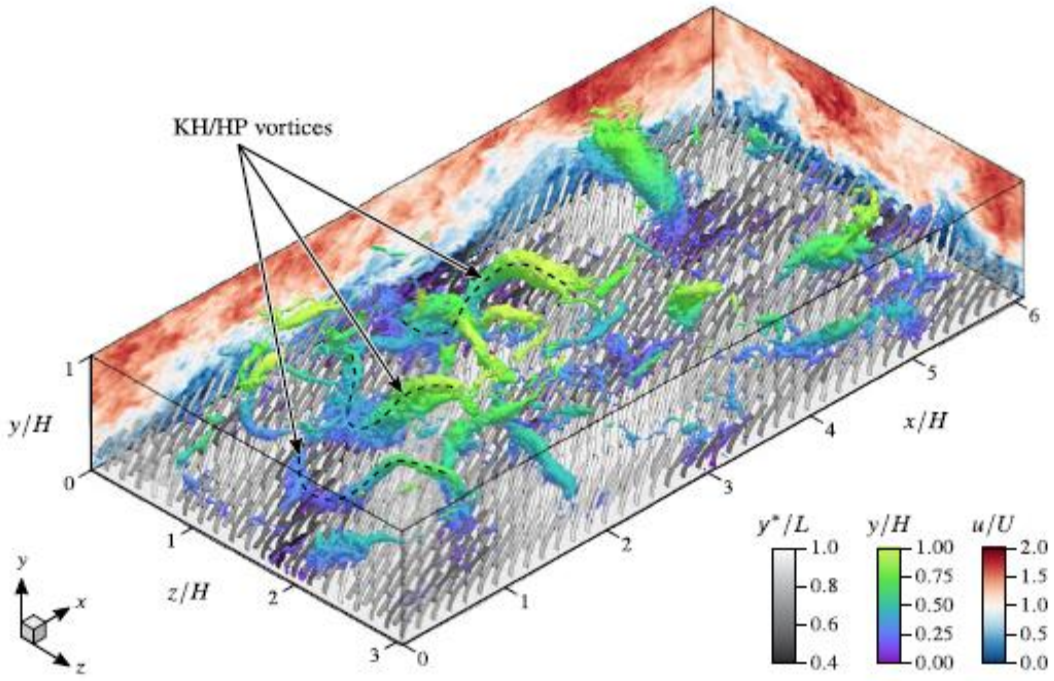

Figure 6. Instantaneous coherent vortex structures in the flow over 800 highly flexible blades in regular arrangement. The vortex structures are visualized by pressure iso-surfaces at certain value and the iso-surfaces are colored by the vertical position. Reproduced from [187], with the permission of Cambridge University Press.

5. Energy harvesting

The interaction of a flexible slender structure with surrounding fluid flow can be utilized to extract energy from ambient flow such as winds, river currents and ocean tides, which are vital sources of renewable energy. One of the major advantages of extracting flow energy from the flow-induced motion of flexible slender structures is that, compared to conventional wind/tidal turbine technology, it can be made very small and portable, so that it is very suitable for charging small-sized, low-power, portable, and remote devices such as unattended sensors or robots.

Flexible slender structures can interact with ambient flow in many ways. Here we restrict ourselves to the configuration where the slender structure is placed in line with the flow. With this configuration, the structure can vibrate under two different types of flow-induced forcing [192]: One is extraneously induced excitation (EIE) where the structure is excited and sustained through external, time-varying flow pressure gradients such as a trail of traveling vortices behind a bluff body; The other is movement-induced excitation (MIE) where the structure is self-excited and self-sustaining through aero-/hydro-elastic instability.

A seminal work in the EIE type was the *energy harvesting eel* proposed by Allen and Smits [193]. They placed a piezoelectric membrane in the wake of a flat plate that was placed perpendicularly to the flow, and used the formed Karman vortex street to induce undulating motion of the membrane as sketched in Figure 1(b1), analogous to the motion of a swimming eel. A number of different membranes, including polyvinylidene fluoride (PVDF), were tested in a water channel at Reynolds number ranging from 5×10^3 to 4×10^4. Their experimental data showed that, as Re increases, the membrane

behaviors tend to be optimal, where the eel undulation frequency matches the natural vortex shedding frequency, i.e. $f_{eel}/f_{nat} \approx 1$. Under this optimal condition, the eel distortion is in synchronization with the convecting vortical structures alternatively shed from the bluff body, and the undulation amplitude is of the order of the bluff body width.

This energy harvesting eel concept was then realized by Taylor et al. [194] through introducing a switched resonant-power conversion circuit to a 24.1-cm long, 7.6-cm wide and 150-μm thick, undulating eel that was made of PVDF layers with multiple electrode pairs. This model was tested in water flows at different speeds, and was able to produce about 2 V output voltage at 0.5 m/s. The same optimal or ideal coupling between the eel undulation and the vortex shedding was confirmed for power extraction. But obvious distortion in both dynamics and power output along the eel length was observed. Pobering and Schwesinger [195] also built a similar but much smaller prototype using a piezoelectric bimorph cantilever of 14-mm long, 11.8-mm wide and 0.35-mm thick, which is clamped in an upstream bluff body of 10.35-mm high. Instead of undulating, the cantilever flutters in its first bending mode, and only produces output voltage of 0.8 V and electrical power of around 0.1 mW in a 45-m/s wind, corresponding to a very low power conversion efficiency. Obviously, the cantilever worked under conditions that are still far from optimal, evidenced by deflection amplitudes of only about tens of micrometers.

Akaydin et al. [196] adopted a slightly different configuration for energy harvesting, in which a piezoelectric beam (30-mm long, 16-mm wide and 0.2-mm thick) is placed with its free end pointing upstream towards a cylinder of diameter 30 mm. When the freestream velocity was tuned such that the vortex shedding frequency matched the resonance frequency of the piezoelectric beam (at $\mathrm{Re} \approx 1.5 \times 10^4$), the beam vibrates violently in its first bending mode. By moving the piezoelectric beam around, the maximum electrical power (at μW level) was obtained when the beam was located with its free end two diameters away from the cylinder and along its centerline.

Instead of from a train of vortices, Wang and Tang [197] studied the energy transfer from a single vortex structure, i.e., a Lamb dipole, to a flexible cantilever. The cantilever has a fixed mass ratio of 1.0 and is placed either along or against the dipole's advection direction. Their simulation results revealed that, when the lateral distance is around the dipole radius, placing the cantilever against the dipole's advection direction is more favorable for energy transfer. With this setting, the cantilever generally experiences two notable increases in its mechanical energy (Figure 7). The first one is caused by the direct impact associated with the dipole's approach, whereas the second one occurs when the dipole just passes by and exerts suction on the cantilever's free end. Each increase leads to a peak, and the second peak is much larger (which symbolizes the maximum transferred energy). At $\mathrm{Re} = 200$, when the lateral distance is about a half of the dipole radius, the cantilever's length is about one dipole radius, and its bending stiffness is moderate, the energy harvesting efficiency can be as high as 10.6%. It was further revealed that this energy transfer process does not change too much over a wide range of Reynolds number.

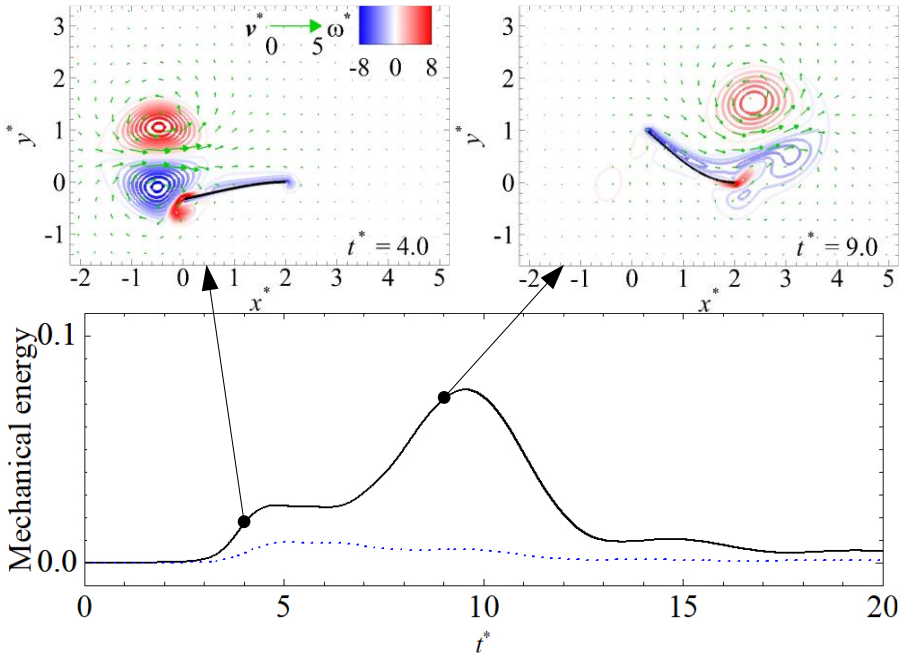

Figure 7. A cantilever interacting with a Lamb dipole. Energy transfer history shows two notable increases when the cantilever is placed against the dipole's advection direction. The first one is caused by the direct impact associated with the dipole's approach (the first inset), whereas the second one occurs when the dipole just passes by and exerts suction on the cantilever's free end (the second inset) (adapted from Wang and Tang [197] with the permission of Elsevier).

In some EIE type energy harvester designs, an appendage was adopted to enhance the FSI and force the connected power-generating cantilever to vibrate with large amplitudes. This type of appendages includes a compliant or revolvable flap in the stalk-leaf architecture (Tan and Panda [198]; Li and Lipson [199]; Bryant and Garcia [200]; Bryant et al. [201]) and a bluff body experiencing flow-induced vibration (Kwon [202]; Akaydin et al. [203]; Gao et al. [204]; Dai et al. [205]). Most of them adopted piezoelectric materials to generate electricity, which has been comprehensively reviewed by Safaei et al. [206].

More studies were conducted on the MIE type energy harvesters. Beyond a certain flow speed, usually known as the critical velocity, negative damping of an elastic structure occurs, which causes divergence of structural deformations（or the classical aeroelastic phenomenon called flutter). Argentina and Mahadevan [207] developed scaling laws for two-dimensional compliant beams in a viscous flow, which showed the relationship between the critical flutter speed U_c, flutter frequency ω and other system parameters as $U_c \sim \left(\frac{Eh^3}{\rho_f L^3}\right)^{\frac{1}{2}}$ and $\omega \sim \left(\frac{\rho_f U^2}{\rho_s hL}\right)^{\frac{1}{2}}$, where U is the freestream velocity. ρ_f and ρ_s are the fluid and beam densities, respectively. h, L and E are the beam thickness, length and elastic modulus, respectively. These scaling laws were then verified by Deivasigamani et al. [208] in three-dimensional, rectangular beams in their wind-tunnel experiments. They indicated that the stiffness of the beam must be low enough or the length of the beam must be long enough so that a realistic critical flutter speed can be obtained.

It has been demonstrated that the MIE flutter is a combination of mode shapes, usually the first and second modes of vibration [209]. This is true if the structure-to-

fluid mass ratio $m^* = \rho_s h/\rho_f L$ is relatively large. For sufficiently small mass ratios, however, the beam flutter motions were governed mainly by fluid added mass and viscous effects, rather than adhering to predicted modal displacements [210].

Three distinct regimes of MIE structure dynamics have been identified, depending on the beam length, stiffness and flow speed [211]: (1) Fixed-point stability, where subsequent to an initial disturbance the system experiences positive damping and the beam returns to a stretched-straight position; (2) Limit-cycle oscillations (LCOs), where MIE flutter eventuates and the beam tip displacements closely resemble a sinusoidal function; and (3) Chaotic flapping, where the flutter is characterized by random snap-through events, large increases in drag and a broad band frequency response. It was also pointed out that maximum bending strain energy was contained in the LCO regime, while energy outputs decreased significantly when the beam transitioned to chaotic flutter (Alben and Shelley [212]; Michelin and Doaré [213]).

The mechanical energy transferred from the flow to the MIE structure can be further converted into electrical energy through various types of power take-off (PTO) mechanisms, such as electromechanical induction, piezoelectricity and triboelectricity. Fei and Li [214] developed the first electromagnetic MIE type harvester. This harvester is composed of a long clamped-clamped polymer film (hence called *windbelt*) of 1.2-m long, 25-mm wide, 0.2-mm thick, and of an electromagnetic converter located just a few dozen of centimeters from one of the membrane's ends. An adjustment system is added to modify the length of the film, which enables it to change the tension of the film and the oscillation frequency. The large surface of this structure enables it to generate 1.3 mW at a low wind speed of 3.1 m/s. In a follow-up study, they further improved the system to generate about 7 mW of electrical power at about 3 m/s wind speed [215].

Using piezoelectric materials, the bending strain energy in fluttering membranes can be converted into electricity, typically in the order of mW. Examples include the aforementioned PVDF based energy harvesting eel developed by Taylor et al. [194] and the piezoelectric bimorph cantilever developed by Pobering and Schwesinger [195], both being the EIE type flutter and operated in flowing water. Taylor et al. [194] further proposed the use of electrostrictive polymers as an alternative to conventional PVDF for the eel due to its much larger piezoelectric conversion efficiency. Other flutter-style piezoelectric energy harvesters operating in air flows were also developed and have been well reviewed by Safaei et al. [206]. Among them, an airfoil-based hybrid harvester design was proposed by Dias et al. [216], Dias et al. [217], which utilized both piezoelectric transduction and electromagnetic induction for power generation.

Electricity can also be generated using the coupling of triboelectrification and electrostatic induction through frequent contact and separation between a fluttering conducting (or dielectric) foil and nearby dielectric (or conducting) plates. By utilizing the wind-induced resonance vibration of a fluorinated ethylene propylene (FEP) film with a surface of nanowire structures between two aluminum plates, Yang et al. [218] demonstrated that a triboelectric nanogenerator (TENG) with a 22-cm long and 2.5-cm wide foil and a 1.25-cm foil-plate gap, which can deliver an output voltage up to 100 V, an output current of 1.6 μA, and a corresponding output power of 0.16 mW under an

external electric load of 100 MΩ, is enough to directly light up tens of commercial light-emitting diodes (LEDs).

In another similar study, Bae et al. [219] found three distinct contact modes between the fluttering foil and the nearby plate, i.e., single-contact mode, double-contact mode and chaotic-contact mode, which are determined by the dimensionless wind speed and the mass ratio of the foil. In this flutter-driven TENG, the flexible foil was made of Au-coated conductive textile, and the rigid counter plate was made of a dielectric PTFE film, leaving a 1-cm separation between them. When the foil is short with dimensions of 7.5-cm length and 5-cm width, it works in the single-contact mode, in which it heavily collides and leaves the counter plate periodically using its trailing edge, similar to a flail with a free-swinging stick or a double pendulum. When the foil is long with dimensions of 12-cm length and 3-cm width, it works in the double-contact mode, where the first contact occurs at the foil's mid-section and propagates with the travelling wave towards the trailing edge, and the second contact then arises at the trailing edge with a much smaller contact strength, after which the foil moves away from the counter plate. The chaotic-contact mode occurs when the wind speed is above a critical speed that is a function of the mass ratio. In this mode, the foil's fluttering motion loses its regularity and becomes random and chaotic, causing very irregular contacts. Their experiments showed that the contacting frequency and the charge collection rate generally increase with the wind speed, but the single-contact mode works much better than the double-contact model. With the short foil, the TENG can deliver a maximum voltage of 250 V and current of 70 mA at a wind speed of 22 m/s. If adopting a dual-plate design, the TENG can delivers an output voltage of up to 200 V and a current of 60 mA with a high frequency of 158 Hz at wind speed of 15 m/s, giving an average power density of approximately 0.86 mW.

In general, conventional wind turbines are not placed in tandem due to adverse wake effects, which cause problems in trailing turbines (loss of power, turbulence-induced vibration, gearbox resonance, etc.). However, flutter harvesters under certain conditions appear to perform beneficially when placed in tandem. The ability to potentially extract more power from a trailing harvester in the wake of another harvester is attractive. However, the benefit decays after three or four harvester-lengths downstream [200]. This phenomenon could allow for more space-efficient designs compared with existing wind farm layouts, such as the matrix-like flutter harvester design (Figure 8) proposed by Pobering and Schwesinger [220]. This is especially useful in highly urban environments, where space is usually considered as a constraint.

In addition to experimental investigations, theoretical and computational models were also developed to predict the energy harvesting performance of fluttering plates/beams. Tang et al. [221] modeled the interactions between a cantilevered flexible plate and its surrounding axial flow using a panel method, i.e., the unsteady lumped vortex model [222]. With this model, they managed to give a breakdown of the total energy transfer between the fluid flow and the plate in different plate sections and in different bending modes. It was found that energy is pumped from the fluid flow into the plate at some locations, while it is transferred from the plate to the fluid flow at other locations. Interestingly, no matter what the structure-to-fluid mass ratio is, energy

is transferred from the plate to the fluid flow at the most downstream section of the plate, corresponding to positive thrust generation. It was also found that, at large mass ratios, the energy transfer occurs largely in the first two bending modes, consistent with the findings reported by Zhang et al. [209]. Moreover, the energy is always transferred from the fluid flow to the plate in the second bending mode. With these understandings obtained, a *flutter-mill* concept was further proposed theoretically that was supposed to operate at large mass ratios and generate electricity using electromagnetic induction. By simply assuming a 10% mechanical-to-electrical energy conversion efficiency without considering the induced electromagnetic force acting on the plate, they compared the flutter-mill with a real horizontal-axis wind turbine and concluded that this theoretical concept can achieve an output capacity comparable to the wind turbine and to operate in the same range of wind speeds.

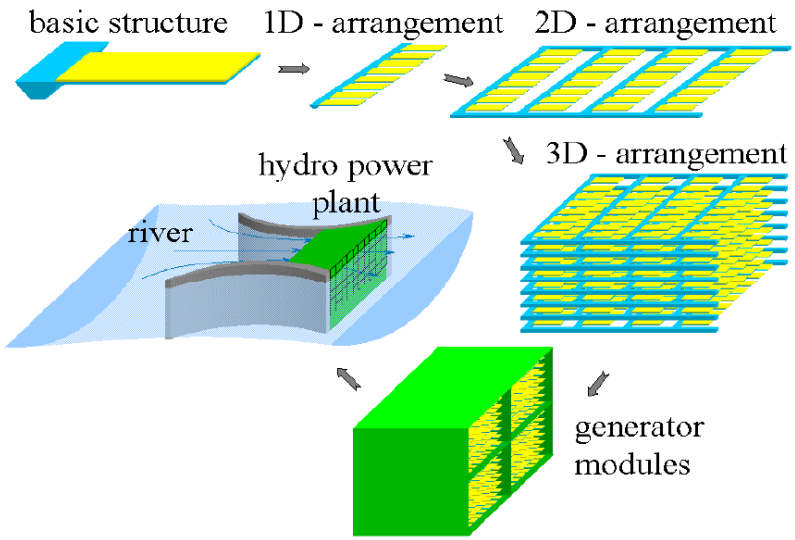

Figure 8. A concept of matrix-like flutter hydropower harvester (adapted from Pobering and Schwesinger [220] with the permission of IEEE).

With a fully coupled fluid-structure-electrical interaction model, Michelin and colleagues (Doaré and Michelin [223]; Michelin and Doaré [213]; Piñeirua et al. [224]) studied the linear stability and dynamics of a fluttering flexible plate that is connected to a dissipative electrical circuit through piezoelectric layers. They found that the number and position of piezoelectric elements play a critical role in energy harvesting performance. The continuous limit was then applied in their model by assuming the piezoelectric material is small compared to the typical wavelength of the plate's deformation. The modeling results suggested that the flow-to-electrical energy conversion is more efficient when the structure-to-fluid mass ratio is small, which can be achieved when the plate's length is long or when the fluid inertia is large compared to the structure's, e.g., in water flows. With small mass ratios, it was found that the optimal location for piezoelectric energy harvesting along the plate is on the downstream half, consistent with the findings reported in Singh et al. [225]. The results also emphasized the importance of the output circuit in the energy transfers: a careful tuning of the circuit characteristic time-scale to that of the fluid-structure oscillations significantly can enhance the conversion efficiency from the structure to the electric

system. Furthermore, the linear stability analyses revealed that the piezoelectric coupling generally stabilized the plate's fluttering modes, and the maximum energy conversion efficiency can be scaled by the square of the piezoelectric coupling coefficient.

6. Outlook

The investigations based on experimental, analytical, and numerical approaches have significantly improved our understanding of the coupling between bio-inspired flexible slender structures and ambient fluid flows. This also expedited the development of new bio-inspired strategies for solving complex problems in various engineering disciplines. Several directions are recommended here for future research endeavors.

Most of the numerical studies focus on two-dimensional problems (planar or cylindrical) and three-dimensional simulations are relatively scarce. From the point of view of real application and basic research, the three-dimensional effect is an indispensable aspect that should be addressed. Three-dimensional simulations usually necessitate large-scale parallel computation. This remains challenging in the sense that some technical difficulties need to be overcome to achieve highly efficient parallel computing.

Whether the best performance in flapping-foil and jellyfish-like swimming can be achieved at structure resonance is an unsolved issue although some clarifications have been made in several recent papers. A more in-depth exploration in this research topic is still needed. The relation between performance and wake resonance is also an open question. The validity of the 'wake resonance argument' in all types of wakes (including drag-producing, thrust-producing and neutral) is questionable.

The symmetry-breaking of wakes is another hot research topic in flapping-foil and jellyfish-like propulsions. Here the term 'symmetry' has slightly different meanings in the two systems. In the case of flapping-foil propulsion, it refers to the spatial-temporal symmetry, while in the case of jellyfish (or cephalopods) propulsion, it refers to the spatial reflection symmetry. For both systems, what triggers the symmetry-breaking instability is largely unknown. In most studies, the stability boundary was determined by physical or numerical experiments. The global stability analysis is a promising method for revealing the physical mechanism behind the symmetry-breaking of the wakes produced by rigid [226] and flexible [227, 228] flapping bodies.

Even though numerous models have been proposed for flagella and cilia, a commonly-accepted one, which can reproduce realistic three-dimensional beating patterns, is still lacking mainly due to the biological complexity. This imposes great challenges on consistently exploring the flagellar or ciliary hydrodynamic performance and the underlying mechanisms of their short- and long-range coordination. Furthermore, in most existing studies the fluid is assumed to be Newtonian. However, more complex fluid environment can be involved in the coordination. For instance, in the mucociliary transport, fluid composed of a low-viscosity periciliary layer and a high-viscosity mucus layer usually exhibits non-Newtonian behaviors, such as the shear-thinning and viscoelastic behaviors. The mechanism of ciliary coordination in such a complex flow is still poorly understood.

In large arrays of wall-mounted flexible structures, the role that passive flexibility plays in the formation of waving motion (i.e., honami or monami) has not been well understood yet. With the advent of more powerful computers, it is now possible to perform simulations that resolve the flows around each individual element (even in the turbulent flow regime). The modal decompositions, such as proper orthogonal decomposition (POD) and dynamic mode decomposition (DMD) which treat the flow and structure together [229], are well-suited tools for revealing the physical mechanism of this mysterious phenomenon.

As for energy harvesting, it should be pointed out that, although promising, so far all the developed flutter-type energy harvesters can only generate small amount of electricity at mW or even μW level. To achieve the power output of 1W level as proposed in the energy-harvesting eel project [194], more efforts are required on efficiency enhancement, prototype scale-up and array arrangement.

Acknowledgements

C.W. gratefully acknowledge the financial support from Departmental General Research Fund (Project No. P0035137) provided by the Department of Mechanical Engineering, The Hong Kong Polytechnic University as well as from Guangdong Basic and Applied Basic Research Foundation (Project No. 2021A1515110749). H.T. would like to acknowledge the financial support from the Research Grants Council of Hong Kong under General Research Fund (Project No. 15214418) and NSFC (Project No. 91952107). X.Z. would like to acknowledge the support from NSFC (Project Nos. 11772338, 11372331, 12172361) and CAS (Project Nos. XDB22040104, XDA22040203).

References

[1]. Hua K and Ferland R J, 2018, Primary cilia proteins: ciliary and extraciliary sites and functions. *Cell. Mol. Life Sci.* **75** 1521-1540.

[2]. Shelley M J and Zhang J, 2011, Flapping and bending bodies interacting with fluid flows. *Annu. Rev. Fluid Mech.* **43** 449-465.

[3]. Wang S, He G, and Zhang X, 2016, Self-propulsion of flapping bodies in viscous fluids: recent advances and perspectives. *Acta Mech. Sin.* **32** 980-990.

[4]. Yu Y, Liu Y, and Amandolese X, 2019, A review on fluid-induced flag vibrations. *Appl. Mech. Rev.* **71**.

[5]. Gursul I and Cleaver D, 2019, Plunging oscillations of airfoils and wings: Progress, opportunities, and challenges. *AIAA J.* **57** 3648-3665.

[6]. Wu X, Zhang X, Tian X, Li X, and Lu W, 2020, A review on fluid dynamics of flapping foils. *Ocean Eng.* **195** 106712.

[7]. Nepf H M, 2012, Flow and transport in regions with aquatic vegetation. *Annu. Rev. Fluid Mech.* **44** 123-142.

[8]. De Langre E, 2008, Effects of wind on plants. *Annu. Rev. Fluid Mech.* **40** 141-168.

[9]. Gosselin F P, 2019, Mechanics of a plant in fluid flow. *J. Exp. Bot.* **70** 3533-3548.

[10]. Brennen C and Winet H, 1977, Fluid mechanics of propulsion by cilia and flagella. *Annu. Rev. Fluid Mech.* **9** 339-398.

[11]. Du Roure O, Lindner A, Nazockdast E N, and Shelley M J, 2019, Dynamics of flexible fibers in viscous flows and fluids. *Annu. Rev. Fluid Mech.* **51** 539-572.

[12]. Gilpin W, Bull M S, and Prakash M, 2020, The multiscale physics of cilia and flagella. *Nat. Rev. Phys.* **2** 74-88.

[13]. Li B-l, Wang Y-w, Yin B, Zhang X, and Zhang X, 2021, Self-propelled swimming of a flexible filament driven by coupled plunging and pitching motions. *J. Hydrodyn.* **33** 157-169.

[14]. https://commons.wikimedia.org/wiki/File:Ocellate_river_stingray,_Boston_Aquarium.jpg.

[15]. https://commons.wikimedia.org/wiki/File:Dragonfly_in_flight_5_(1351481586).jpg.

[16]. https://commons.wikimedia.org/wiki/File:Anguilla_anguilla.jpg.

[17]. Bi X and Zhu Q, 2019, Fluid-structure investigation of a squid-inspired swimmer. *Phys. Fluids*. **31** 101901.

[18]. https://commons.wikimedia.org/wiki/File:Aurelia_aurita_(auge24eu).jpg.

[19]. https://commons.wikimedia.org/wiki/File:Opalescent_inshore_squid.jpg.

[20]. Zhang X, He G, and Zhang X, 2020, Fluid–structure interactions of single and dual wall-mounted 2D flexible filaments in a laminar boundary layer. *J. Fluids Struct.* **92** 102787.

[21]. https://commons.wikimedia.org/wiki/File:Seagrass_Halodule_uninervis_(5777808662).jpg.

[22]. Bottier M, Peña Fernández M, Pelle G, Isabey D, Louis B, Grotberg J B, and Filoche M, 2017, A new index for characterizing micro-bead motion in a flow

induced by ciliary beating: Part II, modeling. *PLoS Comput. Biol.* **13** e1005552.
[23]. Christopher A B, Ochoa S, Krushansky E, Francis R, Tian X, Zahid M, Muñoz R, and Lo C W, 2014, The Effects of Temperature and Anesthetic Agents on Ciliary Function in Murine Respiratory Epithelia. *Front. Pediatr.* **2**.
[24]. Lucas K N, Johnson N, Beaulieu W T, Cathcart E, Tirrell G, Colin S P, Gemmell B J, Dabiri J O, and Costello J H, 2014, Bending rules for animal propulsion. *Nat. Commun.* **5** 1-7.
[25]. Miao J-M and Ho M-H, 2006, Effect of flexure on aerodynamic propulsive efficiency of flapping flexible airfoil. *J. Fluids Struct.* **22** 401-419.
[26]. Yin B and Luo H, 2010, Effect of wing inertia on hovering performance of flexible flapping wings. *Phys. Fluids*. **22** 111902.
[27]. Dai H, Luo H, and Doyle J F, 2012, Dynamic pitching of an elastic rectangular wing in hovering motion. *J. Fluid Mech.* **693** 473-499.
[28]. Shoele K and Zhu Q, 2013, Performance of a wing with nonuniform flexibility in hovering flight. *Phys. Fluids*. **25** 041901.
[29]. Tian F-B, Luo H, Song J, and Lu X-Y, 2013, Force production and asymmetric deformation of a flexible flapping wing in forward flight. *J. Fluids Struct.* **36** 149-161.
[30]. Cleaver D, Calderon D, Wang Z, and Gursul I, 2016, Lift enhancement through flexibility of plunging wings at low Reynolds numbers. *J. Fluids Struct.* **64** 27-45.
[31]. Masoud H and Alexeev A, 2010, Resonance of flexible flapping wings at low Reynolds number. *Phys. Rev. E*. **81** 056304.
[32]. Kang C-K, Aono H, Cesnik C E, and Shyy W, 2011, Effects of flexibility on the aerodynamic performance of flapping wings. *J. Fluid Mech.* **689** 32-74.
[33]. Dewey P A, Boschitsch B M, Moored K W, Stone H A, and Smits A J, 2013, Scaling laws for the thrust production of flexible pitching panels. *J. Fluid Mech.* **732** 29-46.
[34]. Quinn D B, Lauder G V, and Smits A J, 2014, Scaling the propulsive performance of heaving flexible panels. *J. Fluid Mech.* **738** 250-267.
[35]. Katz J and Weihs D, 1978, Hydrodynamic propulsion by large amplitude oscillation of an airfoil with chordwise flexibility. *J. Fluid Mech.* **88** 485-497.
[36]. Zhu Q, 2007, Numerical simulation of a flapping foil with chordwise or spanwise flexibility. *AIAA J.* **45** 2448-2457.
[37]. Heathcote S, Martin D, and Gursul I, 2004, Flexible flapping airfoil propulsion at zero freestream velocity. *AIAA J.* **42** 2196-2204.
[38]. Heathcote S and Gursul I, 2007, Flexible flapping airfoil propulsion at low Reynolds numbers. *AIAA J.* **45** 1066-1079.
[39]. Heathcote S, Wang Z, and Gursul I, 2008, Effect of spanwise flexibility on flapping wing propulsion. *J. Fluids Struct.* **24** 183-199.
[40]. Cleaver D, Gursul I, Calderon D, and Wang Z, 2014, Thrust enhancement due to flexible trailing-edge of plunging foils. *J. Fluids Struct.* **51** 401-412.
[41]. Hua R-N, Zhu L, and Lu X-Y, 2013, Locomotion of a flapping flexible plate. *Phys. Fluids*. **25** 121901.

[42]. Ramananarivo S, Godoy-Diana R, and Thiria B, 2013, Passive elastic mechanism to mimic fish-muscle action in anguilliform swimming. *J R Soc Interface*. **10** 20130667.
[43]. Boyoung, Kim, Sung, Goon, Park, Weixi, Huang, Hyung, Jin, and Sung, 2016, Self-propelled heaving and pitching flexible fin in a quiescent flow. *International Journal of Heat and Fluid Flow*. **62** 273-281.
[44]. Manjunathan S A and Bhardwaj R, 2020, Thrust generation by pitching and heaving of an elastic plate at low Reynolds number. *Phys. Fluids*. **32** 073601.
[45]. Ryu J, Park S G, Huang W-X, and Sung H J, 2019, Hydrodynamics of a three-dimensional self-propelled flexible plate. *Phys. Fluids*. **31** 021902.
[46]. Zhang C, Huang H, and Lu X-Y, 2020, Effect of trailing-edge shape on the self-propulsive performance of heaving flexible plates. *J. Fluid Mech.* **887**.
[47]. Dagenais P and Aegerter C M, 2020, How shape and flapping rate affect the distribution of fluid forces on flexible hydrofoils. *J. Fluid Mech.* **901**.
[48]. Alben S, Witt C, Baker T V, Anderson E, and Lauder G V, 2012, Dynamics of freely swimming flexible foils. *Phys. Fluids*. **24** 051901.
[49]. Paraz F, Schouveiler L, and Eloy C, 2016, Thrust generation by a heaving flexible foil: Resonance, nonlinearities, and optimality. *Phys. Fluids*. **28** 011903.
[50]. David M J, Govardhan R, and Arakeri J, 2017, Thrust generation from pitching foils with flexible trailing edge flaps. *J. Fluid Mech.* **828** 70-103.
[51]. Thiria B and Godoy-Diana R, 2010, How wing compliance drives the efficiency of self-propelled flapping flyers. *Phys. Rev. E*. **82** 015303.
[52]. Ramananarivo S, Godoy-Diana R, and Thiria B, 2011, Rather than resonance, flapping wing flyers may play on aerodynamics to improve performance. *Proc. Natl Acad. Sci.* **108** 5964-5969.
[53]. Alben S, 2008, Optimal flexibility of a flapping appendage in an inviscid fluid. *J. Fluid Mech.* **614** 355-380.
[54]. Michelin S and Llewellyn Smith S G, 2009, Resonance and propulsion performance of a heaving flexible wing. *Phys. Fluids*. **21** 071902.
[55]. Floryan D and Rowley C W, 2018, Clarifying the relationship between efficiency and resonance for flexible inertial swimmers. *J. Fluid Mech.* **853** 271-300.
[56]. Goza A, Floryan D, and Rowley C, 2020, Connections between resonance and nonlinearity in swimming performance of a flexible heaving plate. *J. Fluid Mech.* **888**.
[57]. Fernandez-Feria R and Alaminos-Quesada J, 2021, Analytical results for the propulsion performance of a flexible foil with prescribed pitching and heaving motions and passive small deflection. *J. Fluid Mech.* **910**.
[58]. Sanmiguel-Rojas E and Fernandez-Feria R, 2021, Propulsion enhancement of flexible plunging foils: Comparing linear theory predictions with high-fidelity CFD results. *Ocean Eng.* **235** 109331.
[59]. Zhu X, He G, and Zhang X, 2014, Numerical study on hydrodynamic effect of flexibility in a self-propelled plunging foil. *Comput. Fluids*. **97** 1-20.
[60]. Olivier M and Dumas G, 2016, Effects of mass and chordwise flexibility on 2D

self-propelled flapping wings. *J. Fluids Struct.* **64** 46-66.
[61]. Olivier M and Dumas G, 2016, A parametric investigation of the propulsion of 2D chordwise-flexible flapping wings at low Reynolds number using numerical simulations. *J. Fluids Struct.* **63** 210-237.
[62]. Yeh P D and Alexeev A, 2014, Free swimming of an elastic plate plunging at low Reynolds number. *Phys. Fluids*. **26** 053604.
[63]. Li G, Kemp G, Jaiman R K, and Khoo B C, 2021, A high-fidelity numerical study on the propulsive performance of pitching flexible plates. *Phys. Fluids*. **33** 051901.
[64]. Yeh P D and Alexeev A, 2016, Effect of aspect ratio in free-swimming plunging flexible plates. *Comput. Fluids*. **124** 220-225.
[65]. Zhang Y, Zhou C, and Luo H, 2017, Effect of mass ratio on thrust production of an elastic panel pitching or heaving near resonance. *J. Fluids Struct.* **74** 385-400.
[66]. Castro R F A, Guillamot L, Cros A, and Eloy C, 2014, Non-linear effects on the resonant frequencies of a cantilevered plate. *J. Fluids Struct.* **46** 165-173.
[67]. Triantafyllou G S, Triantafyllou M S, and Grosenbaugh M A, 1993, Optimal thrust development in oscillating foils with application to fish propulsion. *J. Fluids Struct.* **7** 205-224.
[68]. Moored K W, Dewey P A, Smits A, and Haj-Hariri H, 2012, Hydrodynamic wake resonance as an underlying principle of efficient unsteady propulsion. *J. Fluid Mech.* **708** 329-348.
[69]. Moored K W, Dewey P A, Boschitsch B M, Smits A, and Haj-Hariri H, 2014, Linear instability mechanisms leading to optimally efficient locomotion with flexible propulsors. *Phys. Fluids*. **26** 041905.
[70]. Zhu X-J, He G-W, and Zhang X, 2014, Underlying principle of efficient propulsion in flexible plunging foils. *Acta Mech. Sin.* **30** 839-845.
[71]. Arbie M R, Ehrenstein U, and Eloy C, 2016, Stability of momentumless wakes. *J. Fluid Mech.* **808** 316-336.
[72]. Marais C, Thiria B, Wesfreid J E, and Godoy-Diana R, 2012, Stabilizing effect of flexibility in the wake of a flapping foil. *J. Fluid Mech.* **710** 659-669.
[73]. Zhu X, He G, and Zhang X, 2014, How flexibility affects the wake symmetry properties of a self-propelled plunging foil. *J. Fluid Mech.* **751** 164-183.
[74]. Shinde S Y and Arakeri J H, 2014, Flexibility in flapping foil suppresses meandering of induced jet in absence of free stream. *J. Fluid Mech.* **757** 231-250.
[75]. Kim M J and Lee J H, 2019, Wake transitions of flexible foils in a viscous uniform flow. *Phys. Fluids*. **31** 111906.
[76]. Lucas K N, Thornycroft P J, Gemmell B J, Colin S P, Costello J H, and Lauder G V, 2015, Effects of non-uniform stiffness on the swimming performance of a passively-flexing, fish-like foil model. *Bioinspir. Biomim.* **10** 056019.
[77]. Wang W, Huang H, and Lu X-Y, 2020, Optimal chordwise stiffness distribution for self-propelled heaving flexible plates. *Phys. Fluids*. **32** 111905.
[78]. Wang C, Ren F, and Tang H, 2019, Enhancing propulsion performance of a

flexible heaving foil through dynamically adjusting its flexibility. *Bioinspir. Biomim.* **14** 064002.
[79]. Shi G, Xiao Q, and Zhu Q, 2020, Effects of time-varying flexibility on the propulsion performance of a flapping foil. *Phys. Fluids*. **32** 121904.
[80]. Floryan D and Rowley C W, 2020, Distributed flexibility in inertial swimmers. *J. Fluid Mech.* **888**.
[81]. Wang W, Huang H, and Lu X-Y, 2021, Interplay of chordwise stiffness and shape on performance of self-propelled flexible flapping plate. *Phys. Fluids*. **33** 091904.
[82]. Dai L, He G, and Zhang X, 2016, Self-propelled swimming of a flexible plunging foil near a solid wall. *Bioinspir. Biomim.* **11** 046005.
[83]. Park S G, Kim B, and Sung H J, 2017, Hydrodynamics of a self-propelled flexible fin near the ground. *Phys. Fluids*. **29** 051902.
[84]. Dai L, He G, Zhang X, and Zhang X, 2018, Intermittent locomotion of a fish-like swimmer driven by passive elastic mechanism. *Bioinspir. Biomim.* **13** 056011.
[85]. Liu K, Huang H, and Lu X-Y, 2020, Hydrodynamic benefits of intermittent locomotion of a self-propelled flapping plate. *Phys. Rev. E*. **102** 053106.
[86]. Ryu J and Sung H J, 2019, Intermittent locomotion of a self-propelled plate. *Phys. Fluids*. **31** 111902.
[87]. Wang C and Tang H, 2018, Influence of complex driving motion on propulsion performance of a heaving flexible foil. *Bioinspir. Biomim.* **14** 016011.
[88]. Zhu X, He G, and Zhang X, 2014, Flow-mediated interactions between two self-propelled flapping filaments in tandem configuration. *Phys. Rev. Lett.* **113** 238105.
[89]. Uddin E, Huang W-X, and Sung H J, 2015, Actively flapping tandem flexible flags in a viscous flow. *J. Fluid Mech.* **780** 120-142.
[90]. Dai L, He G, Zhang X, and Zhang X, 2018, Stable formations of self-propelled fish-like swimmers induced by hydrodynamic interactions. *J R Soc Interface*. **15** 20180490.
[91]. Godoy-Diana R, Vacher J, Raspa V, and Thiria B, 2019, On the fluid dynamical effects of synchronization in side-by-side swimmers. *Biomimetics*. **4** 77.
[92]. Cong L, Teng B, and Cheng L, 2020, Hydrodynamic behavior of two-dimensional tandem-arranged flapping flexible foils in uniform flow. *Phys. Fluids*. **32** 021903.
[93]. Kurt M, Mivehchi A, and Moored K, 2021, High-Efficiency Can Be Achieved for Non-Uniformly Flexible Pitching Hydrofoils via Tailored Collective Interactions. *Fluids*. **6** 233.
[94]. Ryu J, Byeon H, Lee S J, and Sung H J, 2019, Flapping dynamics of a flexible plate with Navier slip. *Phys. Fluids*. **31** 091901.
[95]. Wang S, Ryu J, He G-Q, Qin F, and Sung H J, 2020, A self-propelled flexible plate with a Navier slip surface. *Phys. Fluids*. **32** 021906.
[96]. Peng J and Alben S, 2012, Effects of shape and stroke parameters on the propulsion performance of an axisymmetric swimmer. *Bioinspir. Biomim.* **7**

016012.
[97]. Alben S, Miller L, and Peng J, 2013, Efficient kinematics for jet-propelled swimming. *J. Fluid Mech.* **733** 100-133.
[98]. Herschlag G and Miller L, 2011, Reynolds number limits for jet propulsion: a numerical study of simplified jellyfish. *J. Theor. Biol.* **285** 84-95.
[99]. Bi X and Zhu Q, 2018, Numerical investigation of cephalopod-inspired locomotion with intermittent bursts. *Bioinspir. Biomim.* **13** 056005.
[100]. Bi X and Zhu Q, 2020, Pulsed-jet propulsion via shape deformation of an axisymmetric swimmer. *Phys. Fluids*. **32** 081902.
[101]. Luo Y, Xiao Q, Zhu Q, and Pan G, 2021, Jet propulsion of a squid-inspired swimmer in the presence of background flow. *Phys. Fluids*. **33** 031909.
[102]. Park S G, Chang C B, Huang W-X, and Sung H J, 2014, Simulation of swimming oblate jellyfish with a paddling-based locomotion. *J. Fluid Mech.* **748** 731-755.
[103]. Park S G, Kim B, Lee J, Huang W-X, and Sung H J, 2015, Dynamics of prolate jellyfish with a jet-based locomotion. *J. Fluids Struct.* **57** 331-343.
[104]. Park S G and Sung H J, 2016, Vortex interaction between two tandem flexible propulsors with a paddling-based locomotion. *J. Fluid Mech.* **793** 612-632.
[105]. Hoover A and Miller L, 2015, A numerical study of the benefits of driving jellyfish bells at their natural frequency. *J. Theor. Biol.* **374** 13-25.
[106]. Hoover A P, Griffith B E, and Miller L A, 2017, Quantifying performance in the medusan mechanospace with an actively swimming three-dimensional jellyfish model. *J. Fluid Mech.* **813** 1112-1155.
[107]. Hoover A P, Porras A J, and Miller L A, 2019, Pump or coast: the role of resonance and passive energy recapture in medusan swimming performance. *J. Fluid Mech.* **863** 1031-1061.
[108]. Dawoodian M and Sau A, 2021, Kinetics and prey capture by a paddling jellyfish: three-dimensional simulation and Lagrangian coherent structure analysis. *J. Fluid Mech.* **912**.
[109]. Luo Y, Xiao Q, Zhu Q, and Pan G, 2020, Pulsed-jet propulsion of a squid-inspired swimmer at high Reynolds number. *Phys. Fluids*. **32** 111901.
[110]. Bi X and Zhu Q, 2019, Dynamics of a squid-inspired swimmer in free swimming. *Bioinspir. Biomim.* **15** 016005.
[111]. Klindt G S, Ruloff C, Wagner C, and Friedrich B M, 2016, Load Response of the Flagellar Beat. *Phys. Rev. Lett.* **117** 258101.
[112]. Ding Y, Nawroth J C, McFall-Ngai M J, and Kanso E, 2014, Mixing and transport by ciliary carpets: a numerical study. *J. Fluid Mech.* **743** 124-140.
[113]. Lindemann C B, 1994, A "Geometric Clutch" Hypothesis to Explain Oscillations of the Axoneme of Cilia and Flagella. *J. Theor. Biol.* **168** 175-189.
[114]. Schoeller S F, Holt W V, and Keaveny E E, 2020, Collective dynamics of sperm cells. *Philos. Trans. R. Soc. Lond., B, Biol. Sci.* **375** 20190384.
[115]. Machemer H, 1972, Ciliary Activity and the Origin of Metachrony in Paramecium: Effects of Increased Viscosity. *J. Exp. Biol.* **57** 239-259.
[116]. Hirokawa N, Okada Y, and Tanaka Y, 2008, Fluid Dynamic Mechanism

Responsible for Breaking the Left-Right Symmetry of the Human Body: The Nodal Flow. *Annu. Rev. Fluid Mech.* **41** 53-72.
[117]. Faubel R, Westendorf C, Bodenschatz E, and Eichele G, 2016, Cilia-based flow network in the brain ventricles. *Science*. **353** 176-178.
[118]. Lyons R A, Saridogan E, and Djahanbakhch O, 2006, The reproductive significance of human Fallopian tube cilia. *Hum. Reprod. Update*. **12** 363-372.
[119]. Ramirez-San Juan G R, Mathijssen A J T M, He M, Jan L, Marshall W, and Prakash M, 2020, Multi-scale spatial heterogeneity enhances particle clearance in airway ciliary arrays. *Nat. Phys.* **16** 958-964.
[120]. Gilpin W, Prakash V N, and Prakash M, 2017, Vortex arrays and ciliary tangles underlie the feeding–swimming trade-off in starfish larvae. *Nat. Phys.* **13** 380-386.
[121]. Shapiro O H, Fernandez V I, Garren M, Guasto J S, Debaillon-Vesque F P, Kramarsky-Winter E, Vardi A, and Stocker R, 2014, Vortical ciliary flows actively enhance mass transport in reef corals. *Proc. Natl Acad. Sci.* **111** 13391.
[122]. Satir P and Christensen S T, 2007, Overview of Structure and Function of Mammalian Cilia. *Annu. Rev. Physiol.* **69** 377-400.
[123]. Chakrabarti B and Saintillan D, 2019, Spontaneous oscillations, beating patterns, and hydrodynamics of active microfilaments. *Phys. Rev. Fluids*. **4** 043102.
[124]. Purcell E M, 1977, Life at low Reynolds number. *Am. J. Phys.* **45** 3-11.
[125]. Bruot N, Kotar J, de Lillo F, Cosentino Lagomarsino M, and Cicuta P, 2012, Driving Potential and Noise Level Determine the Synchronization State of Hydrodynamically Coupled Oscillators. *Phys. Rev. Lett.* **109** 164103.
[126]. Kotar J, Leoni M, Bassetti B, Lagomarsino M C, and Cicuta P, 2010, Hydrodynamic synchronization of colloidal oscillators. *Proc. Natl Acad. Sci.* **107** 7669.
[127]. Ghorbani A and Najafi A, 2017, Symplectic and antiplectic waves in an array of beating cilia attached to a closed body. *Phys. Rev. E*. **95** 052412.
[128]. Uchida N and Golestanian R, 2010, Synchronization and Collective Dynamics in a Carpet of Microfluidic Rotors. *Phys. Rev. Lett.* **104** 178103.
[129]. Kim Y W and Netz R R, 2006, Pumping Fluids with Periodically Beating Grafted Elastic Filaments. *Phys. Rev. Lett.* **96** 158101.
[130]. Eloy C and Lauga E, 2012, Kinematics of the Most Efficient Cilium. *Phys. Rev. Lett.* **109** 038101.
[131]. Guo H, Fauci L, Shelley M, and Kanso E, 2018, Bistability in the synchronization of actuated microfilaments. *J. Fluid Mech.* **836** 304-323.
[132]. Lauga E and Eloy C, 2013, Shape of optimal active flagella. *J. Fluid Mech.* **730** R1.
[133]. Osterman N and Vilfan A, 2011, Finding the ciliary beating pattern with optimal efficiency. *Proc. Natl Acad. Sci.* **108** 15727.
[134]. Guo H, Nawroth J, Ding Y, and Kanso E, 2014, Cilia beating patterns are not hydrodynamically optimal. *Phys. Fluids*. **26** 091901.
[135]. Bayly P V and Dutcher S K, 2016, Steady dynein forces induce flutter instability and propagating waves in mathematical models of flagella. *J R Soc Interface*.

13 20160523.
[136]. De Canio G, Lauga E, and Goldstein R E, 2017, Spontaneous oscillations of elastic filaments induced by molecular motors. *J R Soc Interface*. **14** 20170491.
[137]. Ling F, Guo H, and Kanso E, 2018, Instability-driven oscillations of elastic microfilaments. *J R Soc Interface*. **15** 20180594.
[138]. Jülicher F and Prost J, 1997, Spontaneous Oscillations of Collective Molecular Motors. *Phys. Rev. Lett.* **78** 4510-4513.
[139]. Elgeti J and Gompper G, 2013, Emergence of metachronal waves in cilia arrays. *Proc. Natl Acad. Sci.* **110** 4470.
[140]. Sartori P, Geyer V F, Scholich A, Jülicher F, and Howard J, 2016, Dynamic curvature regulation accounts for the symmetric and asymmetric beats of Chlamydomonas flagella. *eLife*. **5** e13258.
[141]. Woolley D M, Crockett R F, Groom W D I, and Revell S G, 2009, A study of synchronisation between the flagella of bull spermatozoa, with related observations. *J. Exp. Biol.* **212** 2215-2223.
[142]. Riedel Ingmar H, Kruse K, and Howard J, 2005, A Self-Organized Vortex Array of Hydrodynamically Entrained Sperm Cells. *Science*. **309** 300-303.
[143]. Creppy A, Praud O, Druart X, Kohnke P L, and Plouraboué F, 2015, Turbulence of swarming sperm. *Phys. Rev. E*. **92** 032722.
[144]. Pearce D J G, Hoogerbrugge L A, Hook K A, Fisher H S, and Giomi L, 2018, Cellular geometry controls the efficiency of motile sperm aggregates. *J R Soc Interface*. **15** 20180702.
[145]. Gaffney E A, Ishimoto K, and Walker B J, 2021, Modelling Motility: The Mathematics of Spermatozoa. *Front. Cell Dev. Biol.* **9** 1927.
[146]. Brumley D R, Wan K Y, Polin M, and Goldstein R E, 2014, Flagellar synchronization through direct hydrodynamic interactions. *eLife*. **3** e02750.
[147]. Quaranta G, Aubin-Tam M-E, and Tam D, 2015, Hydrodynamics Versus Intracellular Coupling in the Synchronization of Eukaryotic Flagella. *Phys. Rev. Lett.* **115** 238101.
[148]. Wan K Y and Goldstein R E, 2016, Coordinated beating of algal flagella is mediated by basal coupling. *Proc. Natl Acad. Sci.* **113** E2784.
[149]. Geyer V F, Jülicher F, Howard J, and Friedrich B M, 2013, Cell-body rocking is a dominant mechanism for flagellar synchronization in a swimming alga. *Proc. Natl Acad. Sci.* **110** 18058.
[150]. Sleigh M A. 1962, The Biology of Cilia and Flagella. Pergamon.
[151]. Tamm S L and Horridge G A, 1970, The relation between the orientation of the central fibrils and the direction of beat in cilia of Opalina. *Proceedings of the Royal Society of London. Series B. Biological Sciences*. **175** 219-233.
[152]. Hussong J, Breugem W-P, and Westerweel J, 2011, A continuum model for flow induced by metachronal coordination between beating cilia. *J. Fluid Mech.* **684** 137-162.
[153]. Chateau S, D'Ortona U, Poncet S, and Favier J, 2018, Transport and Mixing Induced by Beating Cilia in Human Airways. *Front. Physiol.* **9**.
[154]. Khaderi S N and Onck P R, 2012, Fluid–structure interaction of three-

dimensional magnetic artificial cilia. *J. Fluid Mech.* **708** 303-328.
[155]. Chateau S, Favier J, D'Ortona U, and Poncet S, 2017, Transport efficiency of metachronal waves in 3D cilium arrays immersed in a two-phase flow. *J. Fluid Mech.* **824** 931-961.
[156]. Gueron S, Levit-Gurevich K, Liron N, and Blum J J, 1997, Cilia internal mechanism and metachronal coordination as the result of hydrodynamical coupling. *Proc. Natl Acad. Sci.* **94** 6001-6006.
[157]. Gueron S and Levit-Gurevich K, 1999, Energetic considerations of ciliary beating and the advantage of metachronal coordination. *Proc. Natl Acad. Sci.* **96** 12240.
[158]. Kinosita H and Murakami A, 1967, Control of ciliary motion. *Physiol. Rev.* **47** 53-82.
[159]. Mitran S M, 2007, Metachronal wave formation in a model of pulmonary cilia. *Computers & Structures*. **85** 763-774.
[160]. Han J and Peskin C S, 2018, Spontaneous oscillation and fluid–structure interaction of cilia. *Proc. Natl Acad. Sci.* **115** 4417.
[161]. Wang C, Gsell S, D'Ortona U, and Favier J. 2021. Emergence of metachronal waves in arrays of instability-driven cilia. *The 25th International Congress of Theoretical and Applied Mechanics*.
[162]. Nasouri B and Elfring G J, 2016, Hydrodynamic interactions of cilia on a spherical body. *Phys. Rev. E*. **93** 033111.
[163]. Chakrabarti B, Fürthauer S, and Shelley M J, 2021, A multiscale biophysical model gives quantized metachronal waves in a lattice of cilia. *arXiv preprint arXiv:.01693*.
[164]. Niedermayer T, Eckhardt B, and Lenz P, 2008, Synchronization, phase locking, and metachronal wave formation in ciliary chains. *Chaos*. **18** 037128.
[165]. Solovev A and Friedrich B M, 2020, Global metachronal synchronization and active noise in cilia carpets. *arXiv preprint arXiv:.11741*.
[166]. Loiseau E, Gsell S, Nommick A, Jomard C, Gras D, Chanez P, D'Ortona U, Kodjabachian L, Favier J, and Viallat A, 2020, Active mucus–cilia hydrodynamic coupling drives self-organization of human bronchial epithelium. *Nat. Phys.* **16** 1158-1164.
[167]. Alben S, Shelley M, and Zhang J, 2002, Drag reduction through self-similar bending of a flexible body. *Nature*. **420** 479-481.
[168]. Alben S, Shelley M, and Zhang J, 2004, How flexibility induces streamlining in a two-dimensional flow. *Phys. Fluids*. **16** 1694-1713.
[169]. Zhu L, 2008, Scaling laws for drag of a compliant body in an incompressible viscous flow. *J. Fluid Mech.* **607** 387-400.
[170]. Gosselin F, De Langre E, and Machado-Almeida B A, 2010, Drag reduction of flexible plates by reconfiguration. *J. Fluid Mech.* **650** 319-341.
[171]. Luhar M and Nepf H M, 2011, Flow‐induced reconfiguration of buoyant and flexible aquatic vegetation. *Limnol. Oceanogr.* **56** 2003-2017.
[172]. Barsu S, Doppler D, Jerome J J S, Rivière N, and Lance M, 2016, Drag measurements in laterally confined 2D canopies: reconfiguration and sheltering

effect. *Phys. Fluids*. **28** 107101.
[173]. Leclercq T and de Langre E, 2018, Reconfiguration of elastic blades in oscillatory flow. *J. Fluid Mech.* **838** 606-630.
[174]. Luhar M and Nepf H, 2016, Wave-induced dynamics of flexible blades. *J. Fluids Struct.* **61** 20-41.
[175]. Leclercq T, Peake N, and De Langre E, 2018, Does flutter prevent drag reduction by reconfiguration? *Proc. Math. Phys. Eng.* **474** 20170678.
[176]. Henriquez S and Barrero-Gil A, 2014, Reconfiguration of flexible plates in sheared flow. *Mech. Res. Commun.* **62** 1-4.
[177]. Leclercq T and de Langre E, 2016, Drag reduction by elastic reconfiguration of non-uniform beams in non-uniform flows. *J. Fluids Struct.* **60** 114-129.
[178]. Jin Y, Kim J-T, and Chamorro L P, 2018, Instability-driven frequency decoupling between structure dynamics and wake fluctuations. *Phys. Rev. Fluids*. **3** 044701.
[179]. Jin Y, Kim J-T, Hong L, and Chamorro L P, 2018, Flow-induced oscillations of low-aspect-ratio flexible plates with various tip geometries. *Phys. Fluids*. **30** 097102.
[180]. Jin Y, Kim J-T, Mao Z, and Chamorro L, 2018, On the couple dynamics of wall-mounted flexible plates in tandem. *J. Fluid Mech.* **852**.
[181]. Jin Y, Kim J-T, Fu S, and Chamorro L P, 2019, Flow-induced motions of flexible plates: fluttering, twisting and orbital modes. *J. Fluid Mech.* **864** 273-285.
[182]. Wang S, Ryu J, Yang J, Chen Y, He G-Q, and Sung H J, 2020, Vertically clamped flexible flags in a Poiseuille flow. *Phys. Fluids*. **32** 031902.
[183]. Chen Y, Ryu J, Liu Y, and Sung H J, 2020, Flapping dynamics of vertically clamped three-dimensional flexible flags in a Poiseuille flow. *Phys. Fluids*. **32** 071905.
[184]. Revell A, Mandal P, and Day P, 2016, Application of a lattice Boltzmann-immersed boundary method for fluid-filament dynamics and flow sensing. *J. Biomech.* **49** 2143-2151.
[185]. Favier J, Li C, Kamps L, Revell A, O'connor J, and Brücker C, 2017, The PELskin project—Part I: Fluid–structure interaction for a row of flexible flaps: A reference study in oscillating channel flow. *Meccanica*. **52** 1767-1780.
[186]. O'Connor J and Revell A, 2019, Dynamic interactions of multiple wall-mounted flexible flaps. *J. Fluid Mech.* **870** 189-216.
[187]. Tschisgale S, Löhrer B, Meller R, and Fröhlich J, 2021, Large eddy simulation of the fluid–structure interaction in an abstracted aquatic canopy consisting of flexible blades. *J. Fluid Mech.* **916**.
[188]. Nové-Josserand C, Hebrero F C, Petit L, Megill W, Godoy-Diana R, and Thiria B, 2018, Surface wave energy absorption by a partially submerged bio-inspired canopy. *Bioinspir. Biomim.* **13** 036006.
[189]. Nové-Josserand C, Godoy-Diana R, and Thiria B, 2019, Interference Model for an Array of Wave-Energy-Absorbing Flexible Structures. *Phys. Rev. Appl*. **11** 034054.
[190]. Park S G, 2020, Heat transfer enhancement by a wall-mounted flexible vortex

generator with an inclination angle. *Int. J. Heat Mass Transfer*. **148** 119053.
[191]. Chen Y, Yang J, Liu Y, and Sung H J, 2020, Heat transfer enhancement in a poiseuille channel flow by using multiple wall-mounted flexible flags. *Int. J. Heat Mass Transfer*. **163** 120447.
[192]. McCarthy J, Watkins S, Deivasigamani A, and John S, 2016, Fluttering energy harvesters in the wind: A review. *J. Sound Vib.* **361** 355-377.
[193]. Allen J and Smits A, 2001, Energy harvesting eel. *J. Fluids Struct.* **15** 629-640.
[194]. Taylor G W, Burns J R, Kammann S, Powers W B, and Welsh T R, 2001, The energy harvesting eel: a small subsurface ocean/river power generator. *IEEE J. Oceanic Eng.* **26** 539-547.
[195]. Pobering S and Schwesinger N. 2008. Power supply for wireless sensor systems. *Sensors, 2008 IEEE*.
[196]. Akaydin H D, Elvin N, and Andreopoulos Y, 2010, Energy harvesting from highly unsteady fluid flows using piezoelectric materials. *J. Intell. Mater. Syst. Struct.* **21** 1263-1278.
[197]. Wang C and Tang H, 2019, On the aeroelastic energy transfer from a Lamb dipole to a flexible cantilever. *J. Fluids Struct.* **86** 170-184.
[198]. Tan Y and Panda S. 2007. A novel piezoelectric based wind energy harvester for low-power autonomous wind speed sensor. *IECON 2007-33rd Annual Conference of the IEEE Industrial Electronics Society*.
[199]. Li S and Lipson H. 2009. Vertical-stalk flapping-leaf generator for wind energy harvesting. *ASME 2009 Conference on Smart materials, adaptive structures and intelligent systems*.
[200]. Bryant M and Garcia E, 2011, Modeling and testing of a novel aeroelastic flutter energy harvester. *J. Vib. Acoust.* **133**.
[201]. Bryant M, Wolff E, and Garcia E, 2011, Aeroelastic flutter energy harvester design: the sensitivity of the driving instability to system parameters. *Smart Mater. Struct.* **20** 125017.
[202]. Kwon S-D, 2010, A T-shaped piezoelectric cantilever for fluid energy harvesting. *Appl. Phys. Lett.* **97** 164102.
[203]. Akaydin H, Elvin N, and Andreopoulos Y, 2012, The performance of a self-excited fluidic energy harvester. *Smart Mater. Struct.* **21** 025007.
[204]. Gao X, Shih W-H, and Shih W Y, 2012, Flow energy harvesting using piezoelectric cantilevers with cylindrical extension. *IEEE Trans. Ind. Electron.* **60** 1116-1118.
[205]. Dai H, Abdelkefi A, and Wang L, 2014, Piezoelectric energy harvesting from concurrent vortex-induced vibrations and base excitations. *Nonlinear Dyn.* **77** 967-981.
[206]. Safaei M, Sodano H A, and Anton S R, 2019, A review of energy harvesting using piezoelectric materials: state-of-the-art a decade later (2008–2018). *Smart Mater. Struct.* **28** 113001.
[207]. Argentina M and Mahadevan L, 2005, Fluid-flow-induced flutter of a flag. *Proc. Natl Acad. Sci.* **102** 1829-1834.
[208]. Deivasigamani A, McCarthy J, Watkins S, John S, and Coman F. 2012. Flow-

induced flutter of slender cantilever high-compliance plates. *28th International Congress Of The Aeronautical Sciences, ICAS 2012*.

[209]. Zhang J, Childress S, Libchaber A, and Shelley M, 2000, Flexible filaments in a flowing soap film as a model for one-dimensional flags in a two-dimensional wind. *Nature*. **408** 835-839.

[210]. Yamaguchi N, Yokota K, and Tsujimoto Y, 2000, Flutter limits and behaviors of a flexible thin sheet in high-speed flow—I: analytical method for prediction of the sheet behavior. *J. Fluids Eng.* **122** 65-73.

[211]. Connell B S and Yue D K, 2007, Flapping dynamics of a flag in a uniform stream. *J. Fluid Mech.* **581** 33-67.

[212]. Alben S and Shelley M J, 2008, Flapping states of a flag in an inviscid fluid: bistability and the transition to chaos. *Phys. Rev. Lett.* **100** 074301.

[213]. Michelin S and Doaré O, 2013, Energy harvesting efficiency of piezoelectric flags in axial flows. *J. Fluid Mech.* **714** 489-504.

[214]. Fei F and Li W J. 2009. A fluttering-to-electrical energy transduction system for consumer electronics applications. *2009 IEEE International Conference on Robotics and Biomimetics (ROBIO)*.

[215]. Fei F, Mai J D, and Li W J, 2012, A wind-flutter energy converter for powering wireless sensors. *Sens. Actuators, A*. **173** 163-171.

[216]. Dias J, De Marqui Jr C, and Erturk A, 2013, Hybrid piezoelectric-inductive flow energy harvesting and dimensionless electroaeroelastic analysis for scaling. *Appl. Phys. Lett.* **102** 044101.

[217]. Dias J, De Marqui Jr C, and Erturk A, 2015, Three-degree-of-freedom hybrid piezoelectric-inductive aeroelastic energy harvester exploiting a control surface. *AIAA J.* **53** 394-404.

[218]. Yang Y, Zhu G, Zhang H, Chen J, Zhong X, Lin Z-H, Su Y, Bai P, Wen X, and Wang Z L, 2013, Triboelectric nanogenerator for harvesting wind energy and as self-powered wind vector sensor system. *ACS Nano*. **7** 9461-9468.

[219]. Bae J, Lee J, Kim S, Ha J, Lee B-S, Park Y, Choong C, Kim J-B, Wang Z L, and Kim H-Y, 2014, Flutter-driven triboelectrification for harvesting wind energy. *Nat. Commun.* **5** 1-9.

[220]. Pobering S and Schwesinger N. 2004. A novel hydropower harvesting device. *2004 International Conference on MEMS, NANO and Smart Systems (ICMENS)*.

[221]. Tang L, Païdoussis M P, and Jiang J, 2009, Cantilevered flexible plates in axial flow: energy transfer and the concept of flutter-mill. *J. Sound Vib.* **326** 263-276.

[222]. Tang L and Paı M P, 2007, On the instability and the post-critical behaviour of two-dimensional cantilevered flexible plates in axial flow. *J. Sound Vib.* **305** 97-115.

[223]. Doaré O and Michelin S, 2011, Piezoelectric coupling in energy-harvesting fluttering flexible plates: linear stability analysis and conversion efficiency. *J. Fluids Struct.* **27** 1357-1375.

[224]. Piñeirua M, Doaré O, and Michelin S, 2015, Influence and optimization of the electrodes position in a piezoelectric energy harvesting flag. *J. Sound Vib.* **346** 200-215.

[225]. Singh K, Michelin S, and De Langre E, 2012, The effect of non-uniform damping on flutter in axial flow and energy-harvesting strategies. *Proc. Math. Phys. Eng.* **468** 3620-3635.
[226]. Jallas D, Marquet O, and Fabre D, 2017, Linear and nonlinear perturbation analysis of the symmetry breaking in time-periodic propulsive wakes. *Phys. Rev. E*. **95** 063111.
[227]. Pfister J-L and Marquet O, 2020, Fluid–structure stability analyses and nonlinear dynamics of flexible splitter plates interacting with a circular cylinder flow. *J. Fluid Mech.* **896**.
[228]. Goza A, Colonius T, and Sader J E, 2018, Global modes and nonlinear analysis of inverted-flag flapping. *J. Fluid Mech.* **857** 312-344.
[229]. Goza A and Colonius T, 2018, Modal decomposition of fluid–structure interaction with application to flag flapping. *J. Fluids Struct.* **81** 728-737.